High-intensity exercise training inhibits excessive autophagy in the hyperlipidemic myocardium of ApoE$^{-/-}$ mice via the NAD$^+$-mediated SIRT1/MFN2 pathway

SHAN GAO[1*], WEI YAO[2*], JIN YANG[1], YUJIE LIU[1] and ZUOWEI PEI[1,3]

[1]Department of Central Laboratory, Central Hospital of Dalian University of Technology, Dalian, Liaoning 116033, P.R. China; [2]Department of Ward of Emergency Internal Medicine, Central Hospital of Dalian University of Technology, Dalian, Liaoning 116033, P.R. China; [3]Department of Cardiology, Central Hospital of Dalian University of Technology, Dalian, Liaoning 116033, P.R. China

Received April 7, 2025; Accepted September 25, 2025

DOI: 10.3892/mmr.2025.13753

Abstract. Hyperlipidemia represents a key contributory factor in the development and progression of cardiovascular diseases, contributing to cardiac injury through mechanisms involving oxidative stress, inflammation and autophagic cell death. Nicotinamide adenine dinucleotide (NAD$^+$) serves a critical role in cardiac energy metabolism by supporting mitochondrial function, oxidative phosphorylation and cell stress responses, primarily through the activation of sirtuins (SIRTs). Aerobic exercise training has been demonstrated to enhance cardiovascular function, primarily through the reduction of oxidative stress and inflammatory responses, while also promoting myocardial repair and functional recovery following injury. The present study aimed to explore the protective effects of NAD$^+$ on hyperlipidemia-induced cardiac damage in apolipoprotein E-deficient (ApoE$^{-/-}$) mice. Two mouse models were employed: A cohort of 8-week-old ApoE$^{-/-}$ mice subjected to varying exercise intensities (moderate-intensity continuous and high-intensity interval training) for a 12-week intervention period, and another cohort of 8-week-old ApoE$^{-/-}$ mice divided into four groups [normal diet (ND), ND + NAD$^+$, high-fat diet (HFD) and HFD + NAD$^+$] for a 16-week intervention period. HFD supplemented with 45% fat Kcal% energy feed was used to induce hyperlipidemia. The metabolic data demonstrated that aerobic exercise training elevated myocardial NAD$^+$ levels in hyperlipidemic mice, whereas NAD$^+$ supplementation mitigated elevated lipid levels. Histological and molecular analysis (hematoxylin and eosin staining, wheat germ agglutinin staining, immunohistochemistry, TUNEL and western blotting) revealed that NAD$^+$ alleviated oxidative stress, fibrosis, inflammation and apoptosis. In addition, by activating the SIRT1/mitofusin 2 pathway and enhancing the PI3K/AKT/mTOR pathway, the expression levels of LC3-II and P62 were decreased, indicating enhanced autophagic flux, as the degradation process of autophagosomes fusing with lysosomes was promoted. The present study suggested that NAD$^+$ supplementation could be a promising therapeutic approach to mitigate hyperlipidemia-induced cardiac damage in clinical settings.

Introduction

Hyperlipidemia is a common metabolic disorder, which has been recognized as an independent risk factor for cardiovascular disease (CVD) (1). Individuals with hyperlipidemia have approximately twice the risk of developing CVD compared with those with normal lipid profiles (2). Increasing evidence has suggested that hyperlipidemia causes cardiac damage through oxidative stress, inflammation, pyroptosis and other mechanisms, leading to lipid load-induced dysfunction characterized by myocardial cell death, remodeling, impaired contractility and autophagy-dependent cell death (3-5). Despite the benefits of statins in lowering blood cholesterol levels and preventing CVD, a large number of patients remain at residual risk of CVD events due to intolerance or side effects associated with lipid-lowering medications. Statins and other lipid-lowering agents (e.g., ezetimibe, PCSK9 inhibitors, fibrates, and niacin) can cause adverse effects such as myopathy, liver enzyme elevation, gastrointestinal discomfort, and, in rare cases, new-onset diabetes, which limit their widespread use and patient adherence (6,7). Therefore, further research is needed to identify drugs that can alleviate hyperlipidemia-induced cardiac damage.

As a key intermediate in cellular energy metabolism, nicotinamide adenine dinucleotide (NAD$^+$) participates in numerous biochemical reactions *in vivo* and has garnered widespread scientific interest (8). Studies have shown that NAD$^+$ serves a pivotal role in maintaining redox homeostasis, mitochondrial function and cellular metabolism (9-11).

Correspondence to: Professor Zuowei Pei, Department of Central Laboratory, Central Hospital of Dalian University of Technology, 826 Xinan Road, Dalian, Liaoning 116033, P.R. China
E-mail: pzw_dl@163.com

*Contributed equally

Key words: nicotinamide adenine dinucleotide, hyperlipidemia, cardiac damage, apolipoprotein E-deficient mice, autophagy

In metabolic syndrome, NAD^+ deficiency impairs insulin sensitivity and promotes lipid accumulation (12,13). In heart failure and ischemia-reperfusion injury, NAD^+ enhances mitochondrial biogenesis and limits oxidative stress through the activation of sirtuin (SIRT)1 and SIRT3 (9,14). In arrhythmia, NAD^+ influences calcium handling and electrophysiological stability (15), and in hypertension, it modulates vascular tone by improving endothelial function and reducing inflammation (16). Notably, NAD^+ imbalance is associated with a number of diseases, and is considered a pathogenic factor in numerous human genetic and acquired conditions, including metabolic disorders such as obesity and type 2 diabetes, neurodegenerative diseases such as Alzheimer's and Parkinson's disease, cardiovascular diseases such as heart failure and atherosclerosis, as well as certain cancers (17). Supplementation with NAD^+ has been shown to alleviate the development of heart failure and to potentially influence lifespan through mitochondrial redox regulation (18). NAD^+ also serves a key role in energy metabolism by acting as an essential electron carrier in glycolysis and the tricarboxylic acid cycle, and in cellular repair processes by serving as a substrate for SIRTs and PARPs, which regulate mitochondrial function, DNA repair and stress resistance. Exercise promotes aerobic metabolism and enhances NAD^+ biosynthesis through increased oxidative phosphorylation (14,19). In addition, increased NAD^+ activates signaling pathways related to cardiac protection, such as SIRT1, which promotes the expression of antioxidant enzymes, and decreases oxidative stress and inflammatory responses (20). Furthermore, mitofusin2 (MFN2), an important protein in mitochondrial outer membrane fusion, interacts with SIRT1 to reduce cardiomyocyte autophagy by inhibiting oxidative stress (21). Collectively, these mechanisms facilitate cardiomyocyte repair and regeneration, thereby providing a robust foundation for recovery from cardiac injury.

Exercise of varying intensities induces different levels of NAD^+ enhancement (22). The present study conducted a comparative analysis of moderate-intensity continuous training (MICT) and high-intensity interval training (HIIT) in promoting NAD^+ levels, aiming to elucidate the underlying molecular mechanisms involved. Furthermore, exogenous NAD^+ was administered to explore its mechanism of action. The results of the current study may contribute to an improved understanding of the role and mechanism of aerobic exercise in hyperlipidemia-induced cardiac damage in apolipoprotein E-deficient ($ApoE^{-/-}$) mice by regulating NAD^+ levels.

Materials and methods

Exercise model in mice with hyperlipidemic cardiac damage. A total of 32 male $ApoE^{-/-}$ mice (age, 8 weeks; body weight, 21-25 g) were obtained from Liaoning Changsheng Biotechnology Co., Ltd. The mice were randomly assigned to the following four groups (n=8/group): The control group received a standard chow diet; the high-fat diet (HFD) group was fed HFD alone; the HFD + MICT group received the HFD combined with MICT; and the HFD + HIIT group received the HFD combined with HIIT. The HFD consisted of 60% fat energy from fat feed [cat. no. XSYT-HFD60; Xiaoshu Youtai (Beijing) Biotechnology Co., Ltd.], and the HFD feeding lasted for 12 weeks, followed by 12 weeks of exercise training. All animals were housed in a controlled environment maintained at 24-26˚C with 40-60% relative humidity and a 12-h light/dark cycle, with *ad libitum* access to food and water throughout the study. At the end of the experiment, or when humane endpoints (e.g., severe weight loss >20%, inability to eat or drink, or signs of severe distress), were reached, the mice were euthanized by intraperitoneal injection of pentobarbital sodium at a dose of 150 mg/kg. Death was verified by confirming the complete cessation of heartbeat and respiratory movement, as well as the absence of corneal reflex, in accordance with institutional ethical guidelines. Blood was collected by orbital sinus puncture under anesthesia before sacrifice, with a total volume of ~0.3 ml/mouse, and stored at -80˚C for subsequent analyses. After sacrifice, heart tissues were collected. Some samples were fixed in 10% neutral-buffered formalin at room temperature for 24 h for histological assessment and paraffin embedding, whereas additional samples were snap-frozen in liquid nitrogen for subsequent protein expression analysis via western blotting. All experimental animal procedures were performed in accordance with the Guide for the Management and Use of Laboratory Animals (23) and were approved by the Animal Experiment Committee of the Central Hospital of Dalian University of Technology (Dalian, China; approval no. YN2023-057-55).

Exercise training regimen. $ApoE^{-/-}$ mice in the MICT and HIIT group underwent a treadmill running test to determine maximum running speed using the XR-PT-10B treadmill (Shanghai XinRuan Information Technology Co., Ltd.). The test began at 10 m/min with a 0˚ incline for 20 min, with speed increasing by 4 m/min each min until the mice exhibited signs of exhaustion. In the present study, exhaustion was defined as either i) the mouse remaining stationary on the shock grid for 3 consecutive seconds, or ii) the mouse accumulating a total of 100 electrical stimulations during the running session, regardless of whether it resumed running afterward. This criterion was adopted to avoid excessive exposure to electrical stimulation and to ensure animal welfare by setting a strict upper limit for the number of shocks (24-26). The maximum velocity achieved during exercise was defined as the peak running speed. Before formal training, both groups underwent a standardized 5-min warm-up at 40% of their respective maximum running velocities. The HFD + HIIT group underwent nine sets of high-intensity treadmill exercises, each lasting 1.5 min, with a 1-min rest between sprints, totaling 21.5 min/session at ~85% of maximum running speed. The HFD + MICT group engaged in continuous endurance training at 60% of maximum running speed until matching the HFD + HIIT group distance. After training, both groups had a 5-min flat recovery period at 40% maximum running speed, repeated five times a week for 12 weeks.

NAD^+ therapy model in mice with hyperlipidemic cardiac damage. Male $ApoE^{-/-}$ mice (age, 8 weeks; body weight, 20-25 g) were obtained from Liaoning Changsheng Biotechnology Co., Ltd. A total of 32 mice were used in this study, and these mice were obtained separately from those described in the first subsection. The mice were housed under standard laboratory conditions (24-26˚C, 40-60% humidity, 12-h light/dark cycle). The animals were randomly assigned to the following

four experimental groups (n=6/group): i) Normal diet (ND); ii) ND + NAD^+ (4 mg/kg/day, intraperitoneally); iii) HFD; and iv) HFD + NAD^+ (4 mg/kg/day, intraperitoneally). The intervention period lasted for 16 weeks, during which NAD^+ was administered to the designated groups. HFD was formulated using a commercially available mouse diet enriched with 45%fat Kcal% energy feed (cat. no. MD12032; Jiangsu Medisen Biomedical Co., Ltd.), HFD feeding was continued for 12 weeks followed by 16-week NAD^+ intraperitoneal injection (27). NAD^+ (cat. no. 53-84-9) was purchased from Merck KGaA. Anesthesia was induced using 4% isoflurane in oxygen and maintained at 1.5-2% isoflurane throughout the orbital sinus puncture procedure; all anesthetic protocols were performed in accordance with institutional animal care guidelines. Blood samples were collected from the orbital venous sinus (0.5-0.8 ml/mouse) into serum tubes and immediately centrifuged, with the resulting serum stored at -80˚C for subsequent analysis. At the end of the experiment or when humane endpoints were reached, the mice were euthanized by intraperitoneal injection of pentobarbital sodium at a dose of 150 mg/kg. Death was verified by cessation of heartbeat and respiratory movement, as well as the absence of corneal reflex, in accordance with institutional ethical guidelines. Some of the heart tissues were fixed in 10% formalin for 24 h at room temperature and subsequently embedded in paraffin for histological evaluation. The remaining heart tissue was frozen in liquid nitrogen for western blot analysis. Mice were monitored daily for general health and behavior. Humane endpoints were established to minimize animal suffering, including >20% body weight loss, persistent hunched posture, reduced activity, inability to access food or water, labored breathing or unresponsiveness to stimuli. Animals reaching any of these criteria were humanely euthanized by intraperitoneal injection of pentobarbital sodium. All experimental animal procedures were performed in accordance with the Guide for the Management and Use of Laboratory Animals (23) and were approved by the Animal Experiment Committee of the Central Hospital of Dalian University of Technology (ethics approval no. YN2023-057-55).

Assessment of biochemical parameters. Blood samples were collected from the orbital venous plexus and centrifuged at 854 x g for 10 min at 4˚C using an Eppendorf 5424R centrifuge (Eppendorf SE) to obtain serum. The resulting supernatant (serum) was used for the quantification of a series of biochemical markers. The serum levels of total cholesterol (T-C; cat. no. A111-1-1), triglycerides (TG; cat. no. A110-1-1), and low-density lipoprotein cholesterol (LDL-C; cat. no. A113-1-1) were measured using colorimetric assay kits (Nanjing Jiancheng Bioengineering Institute, Nanjing, China) according to the manufacturer's instructions, and their optical densities (ODs) were read at 500 nm. Oxidative stress parameters were also evaluated using serum samples with the following commercial kits (Nanjing Jiancheng Bioengineering Institute, Nanjing, China), according to the manufacturer's instructions: superoxide dismutase (SOD; cat. no. A001-3-2; OD at 450 nm) and malondialdehyde (MDA; cat. no. A003-1-2; OD at 532 nm). In addition, Levels of coenzyme I NAD(H) were assessed using a specific enzymatic cycling method (cat. no. A114-1-1; Nanjing Jiancheng Bioengineering Institute, Nanjing, China) according to the manufacturer's instructions, and the OD was measured at 570 nm.

In addition, parameters were additionally measured *in vitro* with the following commercial kits (Nanjing Jiancheng Bioengineering Institute, Nanjing, China), according to the manufacturer's instructions: Reduced glutathione (GSH; cat. no. A006-2-1; OD at 405 nm), superoxide dismutase (SOD; cat. no. A001-3-2; OD at 450 nm), total cholesterol (T-C; cat. no. A111-1-1), triglycerides (TG; cat. no. A110-1-1), and low-density lipoprotein cholesterol (LDL-C; cat. no. A113-1-1) were measured using colorimetric assay kits (Nanjing Jiancheng Bioengineering Institute) according to the manufacturer's instructions, and optical densities were read at 500 nm.

All measurements were performed using a calibrated microplate reader and absorbance values were recorded at the specified wavelengths according to the manufacturer's instructions. The use of wavelength-specific detection for each analyte ensured optimal sensitivity and accuracy of the biochemical assays.

Histopathological assessment. Heart tissues were fixed in 10% neutral buffered formalin at 4˚C overnight, followed by sequential dehydration in a graded ethanol series (50, 75, 85, 95 and 100%; 1 h each). Samples were then cleared twice in xylene (12 min each) and embedded in paraffin. Paraffin-embedded cardiac tissues were sectioned at a thickness of 5 μm, and the sections were deparaffinized with xylene (twice for 10 min), rehydrated through a descending ethanol gradient (100, 95, 85 and 75%; 10 min each), and rinsed in PBS three times, with each rinse lasting 5 min.

Subsequently, the sections underwent hematoxylin and eosin (H&E) staining (cat. no. G1120; Beijing Solarbio Technology Co. LTD, Beijing, China), Masson's trichrome staining (cat. no. G1340; Beijing Solarbio Technology Co. LTD.), fluorescein isothiocyanate (FITC)-conjugated wheat germ agglutinin (WGA) staining (cat. no. I3300; Beijing Solarbio Technology Co. LTD, Beijing, China) and TUNEL assay [One-step TUNEL *In Situ* Apoptosis Kit (Green, FITC); cat. no. E-CK-A320; Wuhan Elabscience Biotechnology Co., Ltd.] to evaluate morphological alterations, fibrosis, cell membrane boundaries and apoptosis, respectively. All experiments were performed in accordance with the manufacturers' instructions. After staining, the sections were dehydrated through an ascending ethanol series (75, 85, 95 and 100%; 10 min each), cleared with xylene (twice for 12 min) and mounted with neutral resin. Sections stained with H&E and Masson's trichrome were observed under a BX40 upright light microscope (Olympus Corporation). WGA and TUNEL images were acquired using a STELLARIS 5 laser scanning confocal microscope (Leica Microsystems GmbH).

Periodic acid-Schiff (PAS) staining. PAS staining was performed using Glycogen PAS staining kit (with hematoxylin); cat. no. G1281; Beijing Solarbio Science & Technology Co., Ltd.). Heart tissue fixation and dehydration were performed in the same manner as described above. Sections were then treated with periodic acid solution (0.5%) at room temperature for 5 min to oxidize polysaccharides, followed by two washes in distilled water (1 min each). Slides were incubated with Schiff reagent for 15 min in the dark and washed with

distilled water for 1 min. Nuclei were counterstained with hematoxylin for 1 min. Sections were briefly differentiated in acid alcohol (5 s) and then blued in running water for 10 min or in 1x PBS for 5 min. Sections were dehydrated through a graded ethanol series (75, 85, 95, 100%, 10 min each), cleared in xylene (2x1 min), and mounted with neutral resin. PAS-positive areas, representing polysaccharides, glycogen, mucosubstances, and glycoproteins, appear magenta under light microscopy. Slides were observed and imaged using a BX40 upright light microscope. Staining intensity was graded on a scale of 0-3 (0=negative, 1=weak, 2=moderate, 3=strong), and the percentage of PAS-positive area was graded on a scale of 0-4 (0=<5%, 1=5-25%, 2=26-50%, 3=51-75%, 4=>75%). The final PAS score was obtained by multiplying the two scores, yielding a total score ranging from 0 to 12. Quantitative evaluation was performed by two independent blinded observers in five randomly selected fields of view/section.

Western blotting. Mouse heart tissues frozen at -80˚C were removed from the freezer, and an appropriate amount of tissue was placed in 1.5-ml microcentrifuge tube containing a pre-cooled mixture of protease [and phosphatase inhibitors]. The tissues were cut up on ice, and then broken and cracked by ultrasound with 4˚C ultrasonic crushing for 3 sec and then stop for 3 seconds, a total of 20 sec; power, 30% and 4˚C overnight to extract total proteins. The next day, the samples were centrifuged at 13,700 x g for 10 min at 4˚C, the resulting supernatant was carefully transferred to a fresh 1.5-ml microcentrifuge tube and the volume was recorded. Protein concentration was determined using a bicinchoninic acid assay kit (Beyotime Institute of Biotechnology) in a 96-well plate, alongside a series of gradient standard protein solutions (2, 1, 0.5, 0.25, 0.125 and 0.0625 mg/ml). The absorbance at 562 nm was measured using a microplate reader, and a standard calibration curve was generated for quantification. Equal amounts of protein were then aliquoted into clean 1.5-ml tubes, denatured in a boiling water bath for 5 min, and stored at -80˚C for subsequent use. Equal amounts of protein (10 μg/lane) were separated by SDS-PAGE (10%) and transferred onto polyvinylidene fluoride membranes (Immobilon; MilliporeSigma). The membranes were blocked for 1 h at room temperature in 5% skim milk diluted in Tris-buffered saline-0.1% Tween-20 (TBST) and were subsequently incubated overnight at 4˚C with the following primary antibodies: Rabbit anti-SOD2 (1:5,000; cat. no. K106586P; Beijing Solarbio Science & Technology Co., Ltd.), rabbit anti-heme oxygenase 1 (HO-1; 1:5,000; cat. no. 10701-1-AP; Proteintech Group, Inc.), rabbit anti-SIRT3 (1:1,000; cat. no. 10099-1-AP; Proteintech Group, Inc.), mouse anti-SIRT1 (1:5,000; cat. no. 60303-1-Ig; Proteintech Group, Inc.), rabbit anti-MFN2 (1:5,000; cat. no. 12186-1-AP; Proteintech Group, Inc.), rabbit anti-PI3K p85 (1:1,000; cat. no. 20584-1-AP; Proteintech Group, Inc.), rabbit anti-phosphorylated (p)-PI3K p85 (1:1,000; cat. no. AF3242; Affinity Biosciences), anti-AKT (1:1,000; cat. no. AF0836; Affinity Biosciences), rabbit anti-LC3 II (1:500; cat. no. GB115766; Wuhan Servicebio Technology Co., Ltd.), rabbit anti-P62 (1:5,000; cat. no. 18420-1-AP; Proteintech Group, Inc.), rabbit anti-p-AKT (1:1,000; cat. no. AF0016; Affinity Biosciences), rabbit anti-mTOR (1:1,000; cat. no. AF6308; Affinity Biosciences), rabbit anti-p-mTOR (1:1,000; cat. no. AF3308; Affinity Biosciences), rabbit anti-tubulin β (1:2,000; cat. no. AF7011; all Affinity Biosciences) and mouse anti-β-actin (1:10,000; cat. no. sc-8432; Santa Cruz Biotechnology, Inc.). The next day, the membranes were washed three times in TBST (10 min each) and then incubated for 1 h at room temperature with the appropriate horseradish peroxidase-conjugated secondary antibodies: Anti-rabbit IgG (1:5,000; cat. no. SA00001-2; Proteintech Group, Inc.) or anti-mouse IgG (1:10,000; cat. no. SA00001-1; Proteintech Group, Inc.). Protein bands were visualized [High-sensitivity ECL chemiluminescence detection kit; cat. no. SW134-01; Seven Innovation (Beijing) Biotechnology Co., LTD,] and semi-quantified using ImageJ software (version 1.53t; National Institutes of Health). Tubulin β and β-actin were used as internal loading controls, and relative protein expression levels were normalized accordingly.

Immunohistochemistry. Coronal heart tissue sections were fixed in 10% neutral buffered formalin overnight at 4˚C. The following day, the samples were sequentially dehydrated through a graded ethanol series (50, 70, 85, 90, 95 and 100%, 1 h each), cleared in xylene (twice for 12 min) and embedded in paraffin for histological analysis. Paraffin-embedded tissues were sectioned at a thickness of 5 μm, and were dewaxed twice in xylene (12 min each), rehydrated through a descending ethanol series (100, 95, 85 and 75%, 10 min each), and rinsed in PBS three times for 5 min each. For antigen retrieval, slides were immersed in citrate buffer (pH 6.0) and heated in a microwave oven at high power for 3-5 min, followed by 1-2 min on low power. The slides were then allowed to cool at room temperature for 40 min and rinsed again with PBS (three times, 5 min each). Immunohistochemistry was conducted using a commercial immunohistochemical kit (cat. no. KIT-9720; Fuzhou Maixin Biotech Co., Ltd.). Endogenous peroxidase activity was blocked by incubating the sections with a peroxidase blocking solution for 10 min, followed by three washes with PBS (5 min each). Non-specific binding was blocked by incubating the slides in 5% sheep serum (cat. no. FSP 500; Suzhou Excellent Biotechnology Co., LTD; Suzhou, China) at room temperature for 1 h. After blocking, the sections were incubated overnight at 4˚C with the following primary antibodies: Rabbit anti-SOD (1:100; cat. no. K106586P; Beijing Solarbio Science & Technology Co., Ltd.), rabbit anti-HO-1 (1:100; cat. no. 10701-1-AP; Proteintech Group, Inc.), rabbit anti-SIRT3 (1:100; cat. no. K008232P; Beijing Solarbio Science & Technology Co., Ltd.), rabbit anti-TGF-β1 (1:300; cat. no. 81746-2-RR; Proteintech Group, Inc.), mouse anti-collagen I (1:3,000; cat. no. 67288-1-Ig; Proteintech Group, Inc.), rabbit anti-collagen III (1:1,000; cat. no. 22734-1-AP; Proteintech Group, Inc.), mouse anti-SIRT1 (1:300; cat. no. 60303-1-Ig; Proteintech Group, Inc.), and rabbit anti-MFN2 (1:300; cat. no. 12186-1-AP; Proteintech Group, Inc.).

The following day, the sections were washed three times in PBS (5 min each), then incubated at room temperature for 1 h with HRP-conjugated goat anti-rabbit IgG secondary antibody provided in the N-Histofine Simple Stain Kit (cat. no. KIT-9720; Fuzhou Maixin Biotech Co., Ltd.). Signal development was performed using the metal-enhanced DAB substrate kit (cat. no. DA1015; Beijing Solarbio Science & Technology Co.,

Ltd.) for 10 min at room temperature, followed by rinsing in distilled water. Sections were counterstained with hematoxylin for 1-2 min with room temperature and washed under running tap water for 30 min. Differentiation was carried out in 1% hydrochloric acid ethanol for 3 sec, followed by an additional rinse under running water for 3 min. The stained slides were then dehydrated in ascending concentrations of ethanol (75, 85, 95 and 100%, 10 min each), cleared in xylene twice (12 min each) and mounted with neutral resin. All stained sections were examined using an Olympus BX40 upright light microscope (Olympus Corporation) for morphological analysis was performed using ImageJ software (version 1.53, National Institutes of Health).

KEGG Pathway Analysis. Differentially expressed genes identified from our experiments were subjected to pathway enrichment analysis using the Kyoto Encyclopedia of Genes and Genomes (KEGG) database (kegg.jp/ using the default parameters. Pathways with a P-value <0.05 were considered significantly enriched.

Protein-Protein Interaction (PPI) Network Analysis. Protein-protein interaction (PPI) networks were constructed to explore the potential interactions of SIRT1 with other proteins involved in mitochondrial dynamics and oxidative stress. Analyses were performed using the STRING database (string-db.org/). The list of relevant proteins was uploaded, and interaction scores were calculated using the default medium confidence threshold (0.4). The resulting network was visualized to identify central nodes and functional connections. The potential interactions among PI3K, AKT, and mTOR were investigated using the STRING database (Search Tool for the Retrieval of Interacting Genes/Proteins; string-db.org/). The analysis was performed by inputting the respective gene symbols, with the species limited to *Mus musculus*. A high-confidence interaction score (0.7) was applied as the cutoff. The resulting network was visualized to identify functional associations relevant to myocardial protection.

Tissue-specific expression analysis of MFN2. Tissue-specific expression analysis of MFN2 was performed using publicly available transcriptomic data from the Genotype-Tissue Expression (GTEx) database (accession no. phs000424.v9.p2; gtexportal.org/) and validated with the Human Protein Atlas (HPA; accession no. ENSG00000116688; https://www.proteinatlas.org/ENSG00000116688-MFN2).

Immunofluorescence. Paraffin-embedded tissue sections were deparaffinized, subjected to antigen retrieval and blocked according to the aforementioned standard immunohistochemical procedures. For immunofluorescence staining, the following primary antibodies were applied to the tissue sections: Rabbit anti-SIRT1 (1:100; cat. no. BF0189; Affinity Biosciences) was used for cell staining, mouse anti-SIRT1 (1:300; cat. no. 60303-1-Ig; Proteintech Group, Inc.) was used for double immunofluorescence staining and rabbit anti-MFN2 (1:300; cat. no. 12186-1-AP; Proteintech Group, Inc.). The slides were incubated overnight at 4˚C and washed three times with PBS (5 min each). In the dark, the following appropriate fluorescent secondary antibodies were added for 1 h at room temperature: Alexa Fluor® 488-conjugated anti-rabbit IgG (H+L), $F(ab')_2$ fragment (1:800; cat. no. 4412S; Cell Signaling Technology, Inc.) and Alexa Fluor 594-conjugated anti-mouse IgG (H+L), $F(ab')_2$ fragment (1:800; cat. no. 8890S; Cell Signaling Technology, Inc.). The slides were then washed three times with PBS (5 min each). For nuclear counterstaining, the sections were treated with DAPI (Wuhan Servicebio Technology Co., Ltd.); the slides were washed with PBS three times (5 min each), stained with DAPI for 1 min and rinsed again three times with PBS in the dark. After staining, the sections were mounted using an anti-fade fluorescence mounting medium (Wuhan Servicebio Technology Co., Ltd.), and fluorescence signals were visualized and captured using a Leica TCS SP8 confocal laser scanning microscope (Leica Microsystems GmbH).

Cell culture. The HL-1 mouse cardiomyocyte cell line (cat. no. MYC-TCM783; Dalian Yiran Mingyu Biotechnology Co., Ltd.) was authenticated using short tandem repeat (STR) profiling upon receipt. The STR results confirmed that the cell line used corresponds to HL-1 and does not match the STR profile of C2C12 or any known contaminant cell lines. HL-1 cells exhibit adherent growth characteristics and were cultured in DMEM with high glucose (Gibco; Thermo Fisher Scientific, Inc.) supplemented with 10% fetal bovine serum (Gibco; Thermo Fisher Scientific, Inc.) and 1% penicillin-streptomycin (all Gibco; Thermo Fisher Scientific, Inc.). The cells were maintained in a humidified incubator at 37˚C with 5% CO_2 and 70% relative humidity. Subculturing was performed at a 1:3 ratio when cells reached 80-90% confluence, using standard enzymatic dissociation with 0.25% trypsin-EDTA (Gibco; Thermo Fisher Scientific, Inc.).

Cell passage. Cells were maintained in complete growth medium (DMEM supplemented with 10% fetal bovine serum and 1% penicillin-streptomycin) at 37˚C in a humidified atmosphere containing 5% CO_2. When cultures reached 80-90% confluency, cells were washed twice with phosphate-buffered saline (PBS), detached using 0.25% trypsin-EDTA solution, and collected by centrifugation at 300 x g for 5 min. Cells were resuspended in fresh medium and seeded at an appropriate density for subsequent experiments. Passages were performed every 2-3 days, and only cells within passages 3-10 were used for experiments.

Palmitic acid (PA) Treatment in HL-1 Cells. HL-1 cells were treated with PA; MedChemExpress, Cat. No. HY-N0830) to induce lipotoxicity and mimic metabolic stress in vitro. PA was prepared as a 5 mM stock solution in 0.1 M NaOH and complexed with 10% fatty-acid free bovine serum albumin (BSA) to a final working concentration of 200 μM. Cells were incubated with PA at 37˚C in a 5% CO_2 incubator for 24 h. Following treatment, autophagy markers LC3 II and p62 were assessed by western blotting to evaluate autophagic flux under lipotoxic conditions.

ROS detection. Reactive oxygen species (ROS) levels in adherent cells were measured using the fluorescent probe CM-H2DCFDA (cat no. S0035S, Beyotime Biotechnology Co., Ltd.). CM-H2DCFDA was diluted (1:1,000 in PBS to a

Table I. Small interfering RNA target sequences.

Name	Forward, 5'→3'	Reverse, 5'→3'
ApoE-Mus-217	GCCGUGCUGUUGGUCACAUTT	AUGUGACCAACAGCACGGCTT
ApoE-Mus-415	GCACUGAUGGAGGACACUATT	UAGUGUCCUCCAUCAGUGCTT
ApoE-Mus-1052	GCCAGUGGGCAAACCUGAUTT	AUCAGGUUUGCCCACUGGCTT
Negative control	UUCUCCGAACGUGUCACGUTT	ACGUGACACGUUCGGAGAATT

final concentration of 5 μM. Culture medium was removed, and cells were incubated with sufficient volume of the diluted CM-H2DCFDA to fully cover the cell layer at 37˚C in a CO_2 incubator for 30 min. After incubation, cells were washed three times with PBS to remove excess probe that had not entered the cells. For positive control of ROS production, cells can be stimulated for 20-30 min to achieve a detectable increase in ROS levels. Fluorescence images were captured immediately using a laser-scanning confocal microscope (Leica TCS STELLARIS 5), and signal quantification was performed using ImageJ software (version 1.53).

JC-1 staining for mitochondrial membrane potential. Mitochondrial membrane potential in adherent cells was assessed using the JC-1 fluorescent probe kit ((cat no. C2006, Beyotime Institute of Biotechnology) according to the manufacturer's instructions. Briefly, cells were washed with PBS and incubated with JC-1 staining solution at 37˚C for 20-30 min. Following incubation, cells were washed twice with JC-1 buffer to remove excess dye. Fluorescence images were immediately acquired using a confocal microscope (Leica TCS STELLARIS 5) with excitation/emission settings for JC-1 monomers (green, ~514/529 nm) and aggregates (red, ~585/590 nm). The ratio of red to green fluorescence intensity was quantified using ImageJ software (version 1.53) to assess changes in mitochondrial membrane potential.

EX-527 treatment. HL-1 cardiomyocytes were seeded at a density of $1x10^5$ cells/cm^2 in 10 cm culture dishes and cultured under standard conditions (37˚C, 5% CO_2) until reaching the desired confluency for subsequent experiments. To inhibit SIRT1 activity, cells were treated with 10 μM EX-527 (cat. no. HY-15452; MedChemExpress) for 24 h (37˚C, 5% CO_2). After treatment, the cells were collected for subsequent assays.

Gene silencing via RNA interference. Cells were seeded in 6-cm dishes as in the passage procedure, and the cell confluence was ~60% at the time of transfection. According to the manufacturer's instructions, the ApoE small interfering (si) RNA was used to silence ApoE expression in HL-1 cells using a transfection reagent kit (Lipofectamine 8000; cat no. C0533, Gibco; Thermo Fisher Scientific, Inc.). Cells were transfected with siRNA (20 μM, 37˚C) for 48 h. Culture medium was replaced with fresh medium containing NAD^+, and the cells were incubated for 48 h under standard conditions before subsequent experiments. The efficiency of ApoE knockdown in HL-1 cells was verified by western blotting. Three siRNAs targeting SIRT1 were designed (sequences provided in Table I). HL-1 cells were transfected with 20 μM of each siRNA using Lipofectamine 8000 (Thermo Fisher Scientific) according to the manufacturer's protocol. Knockdown efficiency was assessed by western blot, and ApoE-Mus-415 was used for subsequent experiments. A non-targeting scramble siRNA was used as a negative control. The siRNA target sequences are shown in Table I.

MTS colorimetric cell viability assay. Logarithmic-phase HL-1 cells were collected and resuspended in complete growth medium. Cell concentration was determined using a Cell counter instrument after trypan blue staining to assess cell viability. Based on the counted cell number, the suspension was adjusted to a concentration of $1x10^5$ cells/ml. Subsequently, 100 μl cell suspension was seeded into each well of a 96-well flat-bottom plate. The plate was placed in a humidified incubator at 37˚C with 5% CO_2 for 24 h. When cells had adhered to the well surface, the medium within each insert was gently aspirated following a 4-h incubation in serum-free medium. Subsequently, NAD^+ solutions at varying concentrations (0, 1, 5, 7 and 10 mM) (cat. no. HY-B0445; MedChemExpress) were added to the wells, and the cells were incubated for 48 h in a humidified cell incubator at 37˚C with 5% CO_2. Following treatment, 20 μl MTS reagent (cat. no. G3582; Promega Corporation) was added to each well in the dark. After an additional 2-h incubation, absorbance was measured at 490 nm using a microplate reader. Cell viability under different NAD^+ concentrations was calculated based on OD values at 490 nm. Each experimental condition was performed in triplicate, and all assays were independently repeated three times. Statistical analysis was conducted to evaluate differences between groups.

Statistical analysis. All quantitative data are presented as the mean ± standard error of the mean. Statistical analyses were conducted using SPSS software (version 23.0; IBM Corp.). Intergroup differences were assessed by one-way analysis of variance, followed by Tukey's post hoc test for multiple comparisons. $P<0.05$ was considered to indicate a statistically significant difference.

Results

HIIT enhances NAD^+ metabolism and decreases oxidative stress in $ApoE^{-/-}$ hyperlipidemic mice. The experimental design is shown in Fig. 1A. Significant differences in body weight and heart-to-body weight ratio were observed among the groups (Fig. 1B and C). Mice in the HFD group exhibited the highest body weight and heart-to-body weight ratio, whereas both the

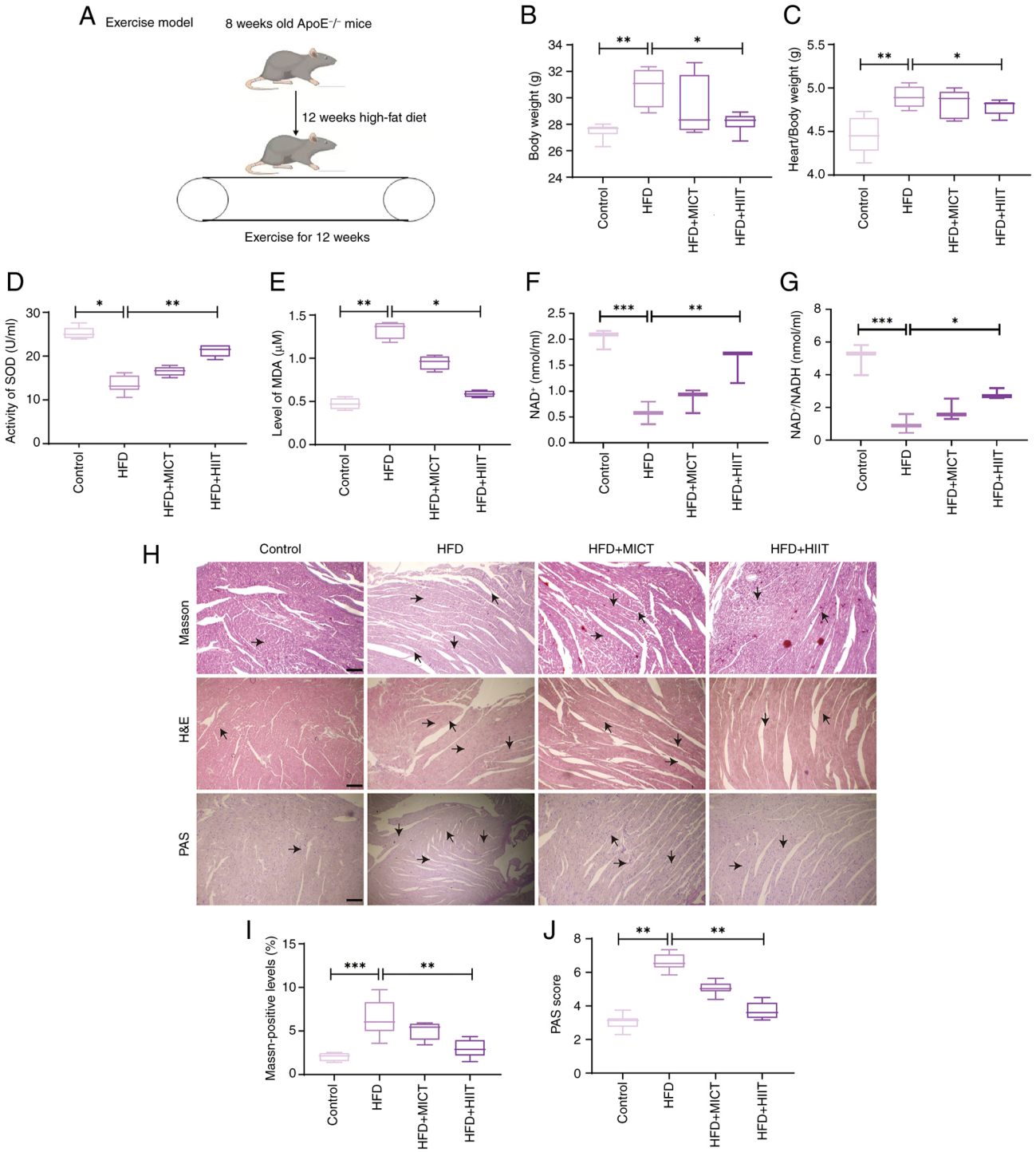

Figure 1. Metabolic data in each group after 12 weeks of exercise training. (A) Schematic diagram of the experimental model. (B) Changes in the body weight of mice. (C) Quantitative analysis of heart/body weight ratio in each group. (D) SOD levels in the serum of mice in each group (n=6). (E) MDA levels in the serum of mice in each group (n=4). Serum (F) NAD^+ and (G) NAD^+/NADH levels in each group of mice (n=3). (H) H&E, Masson and PAS staining heart tissue sections, with arrows indicating positively stained cells. Scale bar, 100 μm; magnification, x40 (n=3). (I) Masson's trichrome staining of myocardial tissue showing collagen deposition. (J) PAS) staining of myocardial tissue showing glycogen deposition. Data are presented as the mean ± standard error of the mean; statistical analysis was performed using one-way ANOVA followed by Tukey's post hoc test. *P<0.05, **P<0.01, ***P<0.001. $ApoE^{-/-}$, apolipoprotein E-deficient; H&E, hematoxylin and eosin; HFD, high-fat diet; HIIT, high-intensity interval training; MDA, malondialdehyde; MICT, moderate-intensity continuous training; NAD^+, nicotinamide adenine dinucleotide; PAS, Periodic acid-Schiff; SOD, superoxide dismutase.

HFD + MICT and HFD + HIIT groups demonstrated reductions in these parameters, with the HFD + HIIT group showing the most pronounced improvement. These findings suggested that HIIT may alleviate HFD-induced obesity and cardiac hypertrophy. Serum analysis showed a significant decrease in SOD activity in the HFD group, which was partially reversed by exercise interventions, with HIIT demonstrating the greatest effect (Fig. 1D). Conversely, MDA levels, which were elevated in the HFD group, were significantly reduced by exercise, particularly following HIIT (Fig. 1E). Furthermore,

in ApoE$^{-/-}$ mice, Exercise increased the NAD+/NADH ratio in both cardiac tissue and serum, with HIIT exerting the most pronounced effect (Fig. 1F and G). Myocardial hypertrophy and fibrosis induced by HFD) were alleviated by exercise, particularly in the HFD + HIIT group, as evidenced by histological analyses. Heart sections were stained with hematoxylin and eosin (H&E) for general morphology, Masson's trichrome for fibrosis, and periodic acid-Schiff (PAS) for glycogen deposition (Fig. 1H and I). PAS staining showed decreased glycogen accumulation in both exercise groups, with the most notable reduction in the HFD + HIIT group (Fig. 1H and J). These results indicated that HIIT provided more pronounced protection against HFD-induced myocardial hypertrophy, fibrosis and glycogen accumulation compared with MICT.

NAD+ supplementation ameliorates HFD-induced obesity, dyslipidemia and oxidative stress. The experimental design is shown in Fig. 2A. Significant differences in body weight and lipid profiles were observed among the groups (Fig. 2B-E). The HFD group showed a pronounced increase in body weight compared with that in the ND group, whereas NAD+ supplementation (HFD + NAD+) significantly lowered body weight, nearing that of the ND group (Fig. 2B). In terms of lipid levels, the HFD group had significantly higher TC, TG, and LDL-C levels compared with those in the ND group. NAD+ supplementation in the HFD + NAD+ group led to a significant decrease in serum lipid levels, including TC), (TG), and (LDL-C), compared with the HFD group (Fig. 2C-E). Immunohistochemistry analysis (Fig. 2F-I) revealed that the ND group exhibited significantly higher expression of SOD, HO-1, and SIRT3 compared with the HFD group. The HFD group showed decreased expression of these markers, whereas the HFD + NAD+ group exhibited increased staining for SOD, HO-1 and SIRT3, similar to the ND group. Semi-quantification of immunohistochemistry results (Fig. 2F-H) confirmed the significantly increased expression of these proteins in the HFD + NAD+ group compared with that in the HFD group. Western blot analysis (Fig. 2J) further supported these findings, showing a marked increase in SOD, HO-1 and SIRT3 expression in the HFD + NAD+ group compared with those in the HFD group. Semi-quantitative analysis of western blotting data confirmed the enhanced expression of these proteins in the NAD+ supplemented group. Notably, NAD+ supplementation did not produce significant effects in mice fed a ND.

NAD+ supplementation attenuates myocardial fibrosis and extracellular matrix (ECM) remodeling in HFD-induced mice. Masson's trichrome staining (Fig. 3A) revealed substantial collagen deposition in the HFD group, indicative of fibrosis, while NAD+ supplementation (HFD + NAD+) reduced this deposition to levels similar to those in the ND group. Immunohistochemical staining of the fibrosis-related markers TGF-β, collagen I and III (Fig. 3B-D) exhibited elevated expression in the HFD group, which was markedly reduced in response to NAD+ supplementation, approaching the levels observed in the ND group. H&E staining (Fig. 3E) demonstrated structural disorganization and injury in the HFD group, whereas NAD+ supplementation improved myocardial architecture, especially in the HFD + NAD+ group. WGA staining (Fig. 3F) confirmed enhanced myocardial cell integrity in both the ND + NAD+ and HFD + NAD+ groups. Semi-quantitative analysis further confirmed that NAD+ supplementation significantly reduced the Masson-positive area, and TGF-β, collagen I and collagen III expression (Fig. 3G-J) levels, indicating a protective effect against myocardial fibrosis and ECM remodeling in the HFD + NAD+ group. Notably, NAD+ supplementation did not induce significant changes in the ND group, suggesting that its protective effects are specific to pathological conditions such as HFD-induced cardiac injury.

NAD+ ameliorates cardiac damage in hyperlipidemic mice via the SIRT1/MFN2 pathway. KEGG pathway analysis (Fig. S1) indicated that SIRT1 serves a central role in regulating key pathways involved in cellular metabolism and stress response. Protein interaction analysis (Fig. 4A) highlighted potential interactions between SIRT1 and MFN2 involved in mitochondrial dynamics and oxidative stress. Tissue specificity analysis of MFN2 (Fig. S2) revealed its predominant expression in myocardial tissue, suggesting its critical role in cardiac function. Western blot analysis (Fig. 4B) showed that SIRT1 and MFN2 protein expression levels were significantly reduced in the HFD group compared with those in the ND group. However, NAD+ supplementation (HFD + NAD+) restored the expression of both SIRT1 and MFN2 to levels comparable with the HFD group, suggesting that NAD+ exerts protective effects by modulating these proteins. Immunohistochemical staining (Fig. 4C) further confirmed that SIRT1 and MFN2 expression levels were reduced in the HFD group, with marked restoration in the HFD + NAD+ group. The arrows in the staining images indicate areas of stained cells, illustrating the cellular localization of these proteins in myocardial tissue. Additionally, immunofluorescence double-labeling colocalization staining (Fig. 4D) showed clear colocalization of SIRT1 and MFN2 in the heart tissue, confirming that NAD+ supplementation enhanced the expression of both proteins in myocardial cells. Notably, NAD+ administration did not significantly affect SIRT1 or MFN2 expression in the ND group, reinforcing that its modulatory effects are specific to pathological conditions such as HFD-induced cardiac stress.

HIIT regulates the myocardial PI3K/AKT/mTOR pathway through NAD+-induced regulation of the SIRT1/MFN2 pathway. TUNEL staining (Fig. 5A) revealed increased myocardial apoptosis in the HFD group, which was markedly reduced by NAD+ supplementation in the HFD + NAD+ group, indicating enhanced cell survival. Protein interaction analysis (Fig. 5B) identified key interactions between PI3K, AKT and mTOR, suggesting their involvement in myocardial protection. Western blot analysis (Fig. 5C) confirmed these findings, showing decreased p-PI3K/PI3K and p-AKT/AKT levels but elevated p-mTOR/mTOR levels in the HFD group. Notably, NAD+ supplementation restored PI3K and AKT phosphorylation while suppressing the abnormal increase in p-mTOR expression. In addition, in the HFD group, both LC3 II and P62 levels were increased, suggesting impaired autophagic flux (Fig. S3A). By contrast, in the HFD + NAD+ group, the levels of LC3 II and p62 were decreased, indicating restoration of autophagic degradation and enhanced autophagic flux following NAD+ supplementation, as decreased accumulation of both LC3 II and p62 reflects improved turnover

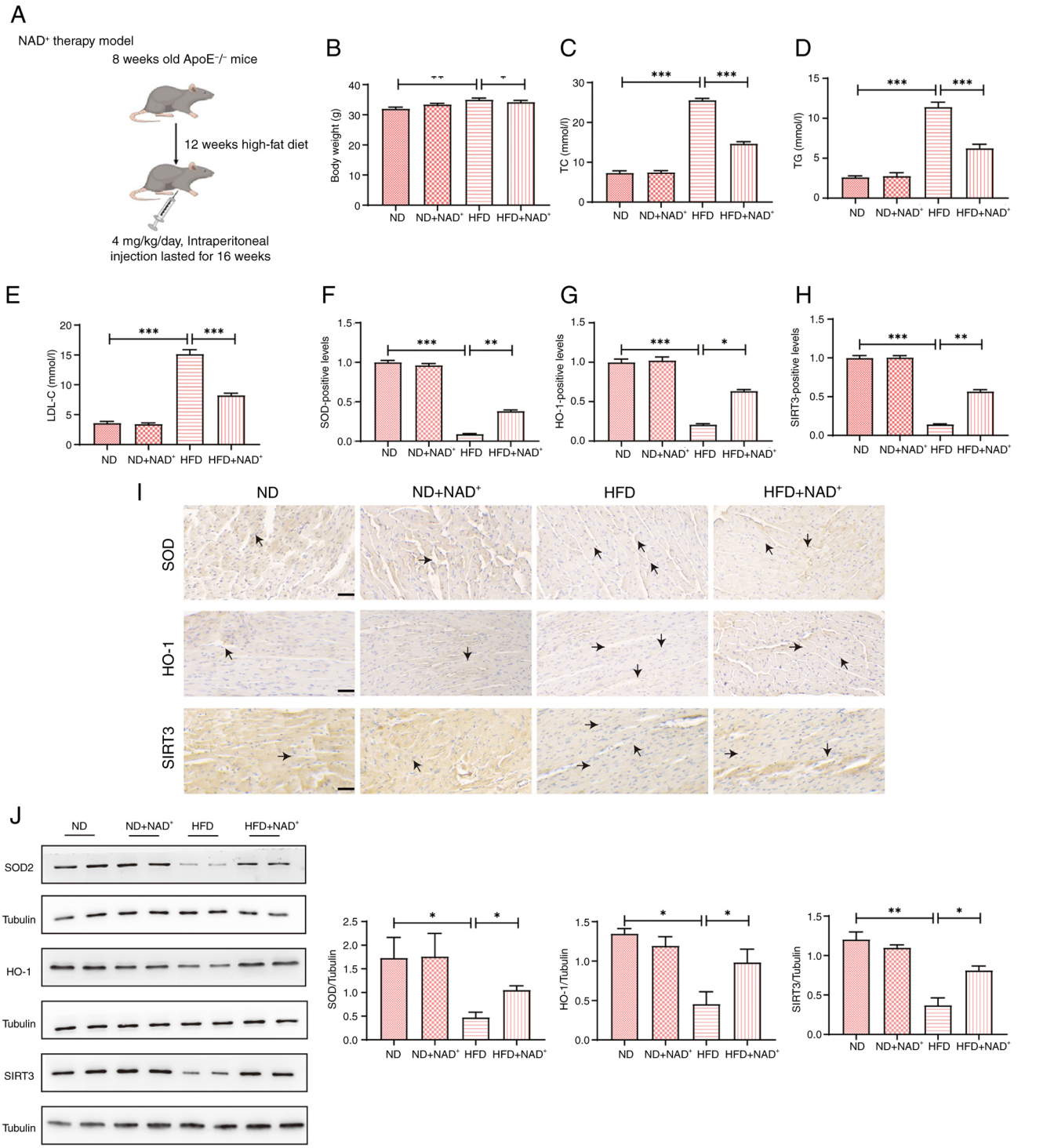

Figure 2. Effects of NAD+ supplementation on body weight, lipid profiles and antioxidant proteins in HFD-induced mice. (A) Schematic diagram of the experimental model. (B) Body weight changes in the ND, ND + NAD+, HFD and HFD + NAD+ groups. Lipid profiles of the mice in all groups, including (C) TC, (D) TG and (E) LDL-C (n=6). Semi-quantification of immunohistochemical results showing significant upregulation of (F) SOD, (G) HO-1 and (H) SIRT3 in the HFD + NAD+ compared with in the HFD group (n=4). (I) Immunohistochemical staining of the antioxidant proteins SOD, HO-1 and SIRT3 in heart tissue; arrows indicate positively stained cells. Magnification, x40; scale bar, 100 μm (n=3). (J) Western blot analysis of SOD, HO-1 and SIRT3 expression in heart tissue, and semi-quantification of western blotting data, confirming increased expression of SOD, HO-1 and SIRT3 in the HFD + NAD+ group. Data are presented as the mean ± standard error of the mean; statistical analysis was performed using one-way ANOVA followed by Tukey's post hoc test. *P<0.05, **P<0.01, ***P<0.001. ApoE$^{-/-}$, apolipoprotein E-deficient; HFD, high-fat diet; HO-1, heme oxygenase 1; LDL-C, low-density lipoprotein cholesterol; NAD+, nicotinamide adenine dinucleotide; ND, normal diet; SIRT3, sirtuin 3; SOD, superoxide dismutase; TC, total cholesterol; TG, triglycerides.

of autophagosomes rather than impaired autophagosome formation. These results suggested that NAD+ exerts cardioprotective effects through activation of the PI3K/AKT/mTOR pathway and increased autophagy by promoting autophagic flux. Notably, NAD+ treatment did not significantly affect apoptosis markers or autophagy-related proteins in the ND group, suggesting that its beneficial effects are specific to the pathological state induced by HFD.

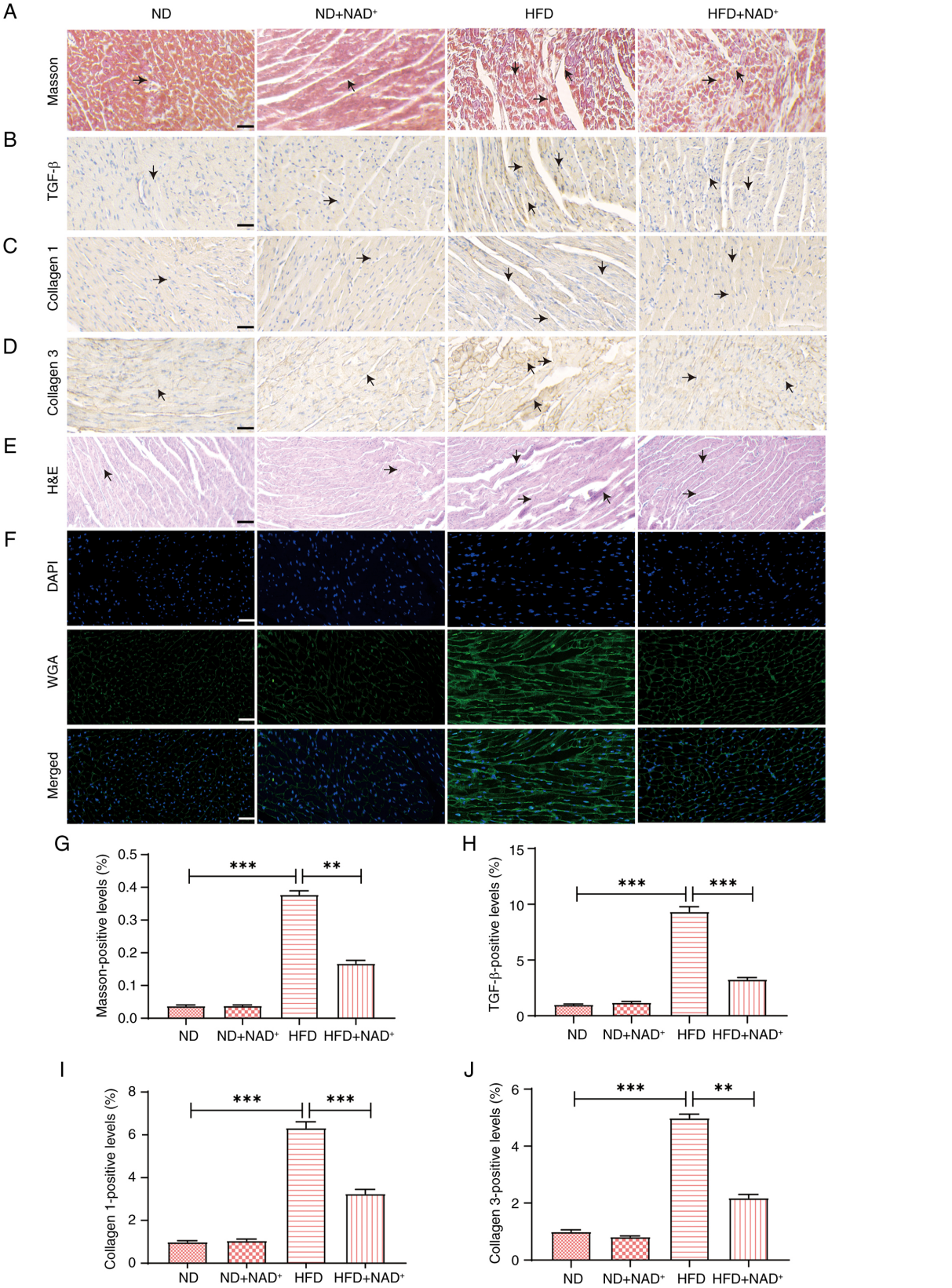

Figure 3. NAD+ supplementation attenuates myocardial fibrosis and ECM remodeling in HFD-induced mice. (A) Masson's trichrome staining of myocardial tissue. Blue-stained regions indicate collagen deposition (fibrotic areas), and red indicates myocardial fibers. Black arrows point to areas of increased collagen accumulation. Scale bar, 100 μm. Immunohistochemical staining of fibrosis-related markers: (B) TGF-β, (C) collagen I, and (D) collagen III. Brown staining indicates positive expression, and black arrows highlight regions with enhanced marker expression. Scale bar, 100 μm. (E) H&E staining of myocardial tissue showing general histological structure. Black arrows indicate areas of myocardial hypertrophy or structural abnormalities. Scale bar, 100 μm. (F) WGA staining showing improved myocardial cell integrity in the HFD + NAD+ group. Scale bar, 100 μm. Semi-quantification of the (G) Masson-positive area, and (H) TGF-β, (I) collagen I and (J) collagen III levels. NAD+ supplementation significantly reduced fibrosis and ECM remodeling in the HFD + NAD+ group compared with in the HFD group. Data are presented as the mean ± standard error of the mean, n=3; statistical analysis was performed using one-way ANOVA followed by Tukey's post hoc test. **P<0.01, ***P<0.001. ECM, extracellular matrix; H&E, hematoxylin and eosin; HFD, high-fat diet; NAD+, nicotinamide adenine dinucleotide; ND, normal diet; WGA, what germ agglutinin.

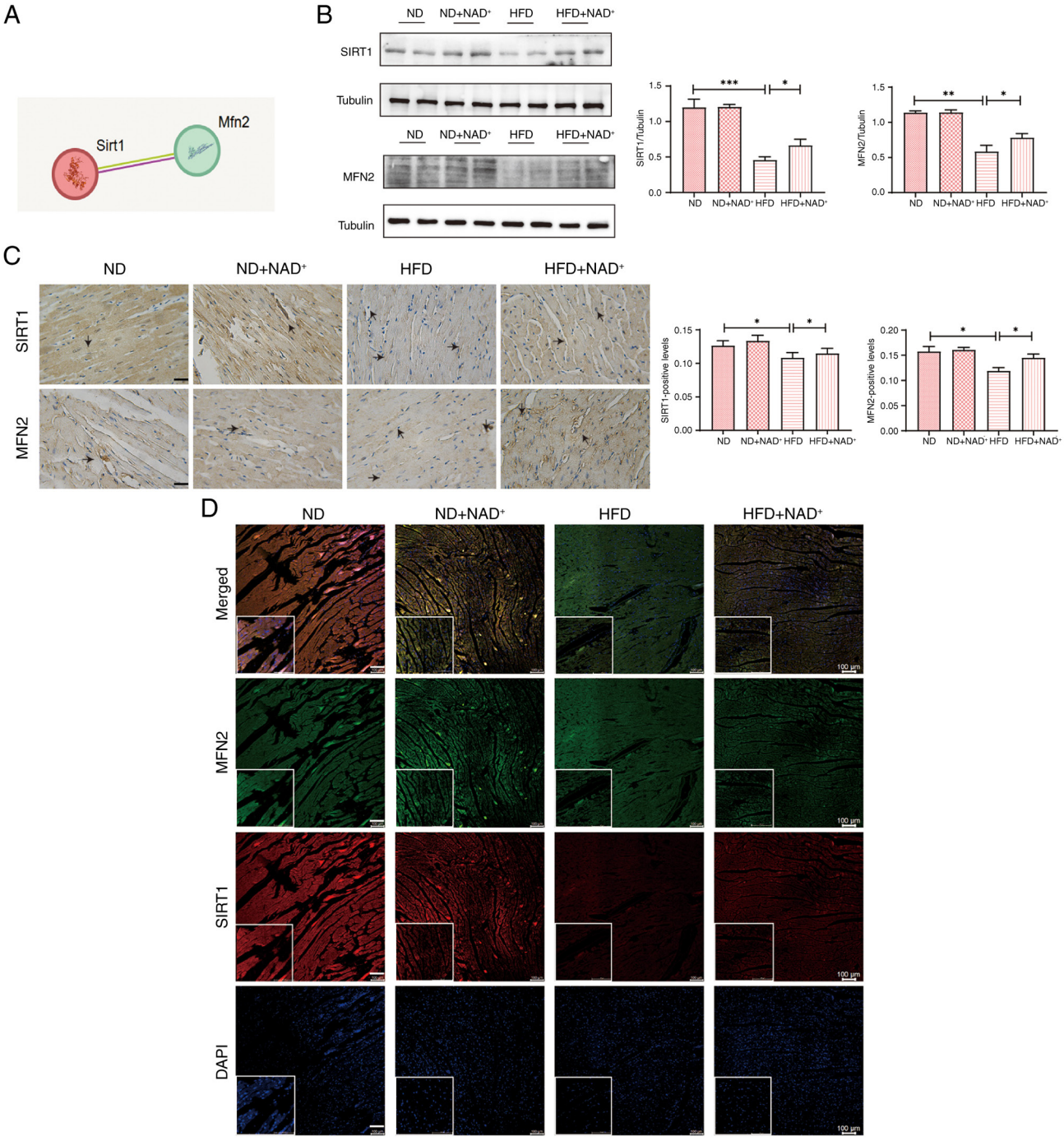

Figure 4. NAD$^+$ ameliorates cardiac damage in hyperlipidemic mice by modulating the SIRT1/MFN2 pathway. (A) Protein interaction analysis. (B) Expression levels of SIRT1 and MFN2 proteins in the heart tissues of mice. (C) Representative immunohistochemistry images showing the expression of SIRT1 and MFN2 in myocardial tissue. The arrows indicate areas of stained cells. Scale bar, 100 μm; magnification, x40. (D) SIRT1 and MFN 2 were detected by immunofluorescence double staining to assess colocalization. Scale bars, 100 and 50 μm; magnification, x40. Data are presented as the mean ± standard error of the mean (n=3); statistical analysis was performed using one-way ANOVA followed by Tukey's post hoc test. *P<0.05, **P<0.01, ***P<0.001. HFD, high-fat diet; MFN2, mitofusin 2; NAD$^+$, nicotinamide adenine dinucleotide; ND, normal diet; SIRT1, sirtuin 1.

NAD$^+$ protects ApoE$^{-/-}$ HL-1 cells from lipid accumulation and oxidative stress. Western blot analysis confirmed successful knockdown of ApoE expression in HL-1 cardiomyocytes following transfection with ApoE-specific siRNA (Fig. S4). NAD$^+$ treatment at concentrations of 1, 5 and 7 μM significantly improved cell viability compared with the control group, with 5 μM showing the most pronounced effect (Fig. 6A). By contrast, 10 μM NAD$^+$ did not significantly affect viability compared with the control. In the ApoE$^{-/-}$ group, lipid accumulation was evident, as indicated by elevated TC (Fig. 6B), TG (Fig. 6C) and LDL-C (Fig. 6D) levels, which were significantly reduced by NAD$^+$ supplementation (ApoE$^{-/-}$ + NAD$^+$ group). Additionally, NAD$^+$ treatment increased GSH levels (Fig. 6E) and enhanced SOD activity (Fig. 6F), indicating improved antioxidant capacity. ROS) staining (Fig. 6G) showed increased ROS accumulation in the ApoE$^{-/-}$ group, which was mitigated by NAD$^+$ treatment. Microscopic images (Fig. 6H) confirmed that NAD$^+$ supplementation

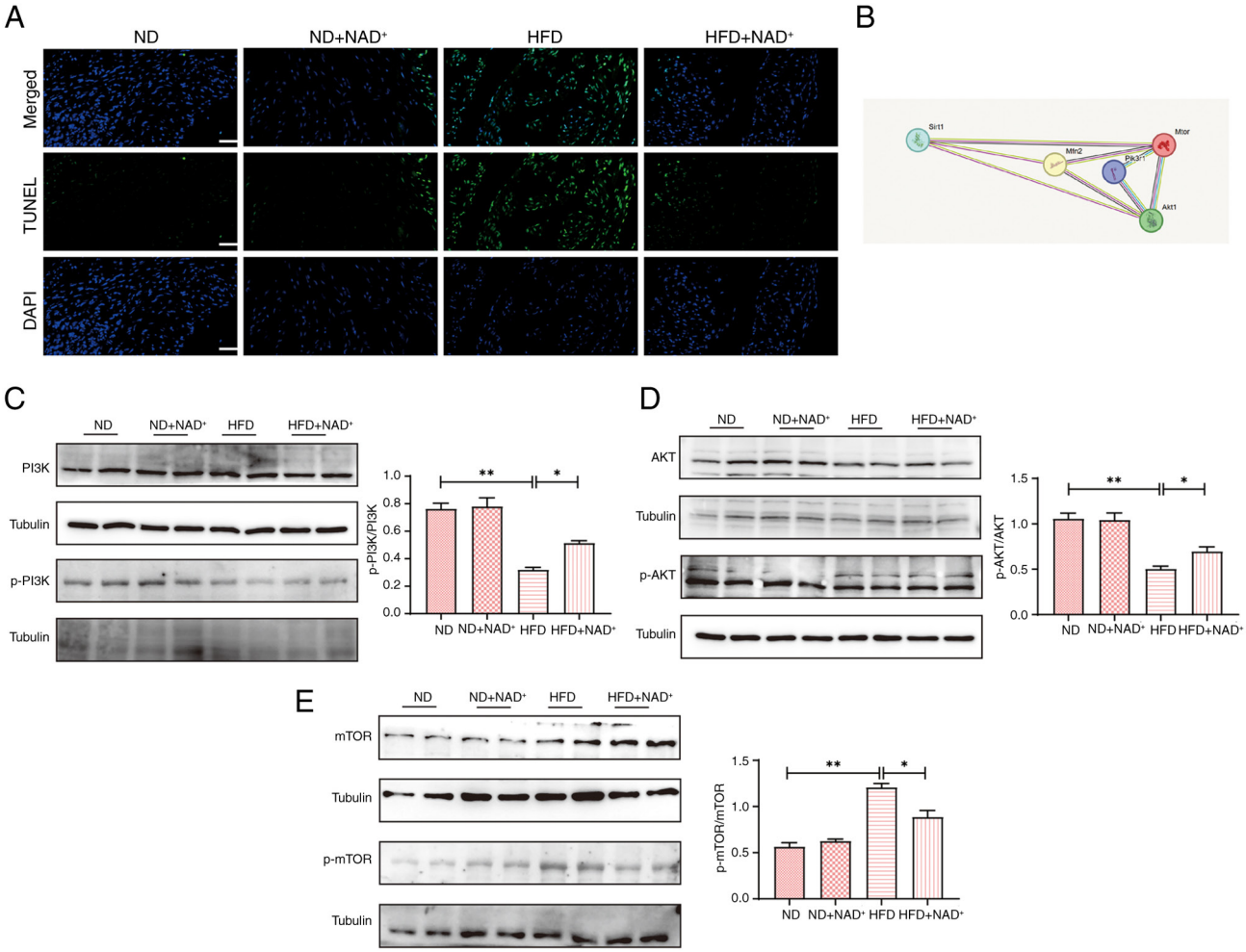

Figure 5. NAD+ supplementation activates the PI3K/AKT/mTOR pathway in the myocardium. (A) TUNEL staining was performed to assess myocardial cell apoptosis in the heart tissues of mice. Magnification, x40; scale bar, 100 μm. (B) Protein interaction analysis. Expression levels of (C) p-PI3K/PI3K, (D) p-AKT/AKT and (E) p-mTOR/mTOR in the heart tissues of mice. Data are presented as the mean ± standard error of the mean (n=4); statistical analysis was performed using one-way ANOVA followed by Tukey's post hoc test. *P<0.05, **P<0.01. HFD, high-fat diet; Mfn2, mitofusin 2; NAD+, nicotinamide adenine dinucleotide; ND, normal diet; p-, phosphorylated; Sirt1, sirtuin 1.

improved cell morphology and viability, as evidenced by more uniform cell shape, increased adherence and reduced cell shrinkage and detachment compared with the untreated group. Immunofluorescence staining (Fig. 6J) showed increased expression of SIRT1 in the ApoE$^{-/-}$ + NAD+ group, suggesting NAD+ activation of the SIRT1 pathway compared with ApoE$^{-/-}$ group. JC-1 staining (Fig. 6I) revealed improved mitochondrial membrane potential in the ApoE$^{-/-}$ + NAD+ group compared with ApoE$^{-/-}$ group, indicating enhanced mitochondrial function with NAD+ treatment. These findings demonstrate that NAD+ supplementation may improve cellular function, lipid metabolism and oxidative stress in HL-1 cells. Notably, NAD+ had minimal effects on lipid levels, antioxidant capacity and mitochondrial function in untransfected control cells, suggesting that its beneficial effects are specific to ApoE$^{-/-}$-induced cellular stress.

NAD+ enhances the SIRT1/MFN2 pathway to protect ApoE$^{-/-}$ HL-1 cells through SIRT1 upregulation. Fig. 7A shows representative immunofluorescence images of MFN2 and SIRT1 double staining, with colocalization observed in the cytoplasm of cells, particularly in the ApoE$^{-/-}$+NAD+ group, indicating that NAD+ treatment promoted the co-expression of these proteins. Furthermore, western blot analysis showed increased levels of both MFN2 and SIRT1 in the ApoE$^{-/-}$ + NAD+ group compared with those in the ApoE$^{-/-}$ group, further supporting the immunofluorescence results (Fig. 7B). Additionally, activation of the PI3K/AKT pathway was observed in the ApoE$^{-/-}$ + NAD+ group, indicated by restored phosphorylation of PI3K and AKT and suppression of the HFD-induced increase in p-mTOR, compared with the ApoE$^{-/-}$ group. To further validate the involvement of autophagy *in vitro*, HL-1 cells were treated with PA), and the levels of LC3 II and P62 were assessed. Consistent with the *in vivo* findings, PA treatment led to a significant accumulation of both LC3 II and P62, suggesting impaired autophagic flux (Fig. S3B). However, NAD+ markedly reduced the levels of LC3 II and P62 in PA-treated cells, indicating that NAD+ supplementation may restore autophagic degradation and enhance autophagic flux under lipotoxic stress conditions. To determine whether NAD+ supplementation activated SIRT1 rather than merely increased its expression, HL-1 cells were treated with PA and co-incubated with NAD+ and/or the SIRT1 inhibitor EX-527. NAD+ treatment significantly increased SIRT1 expression

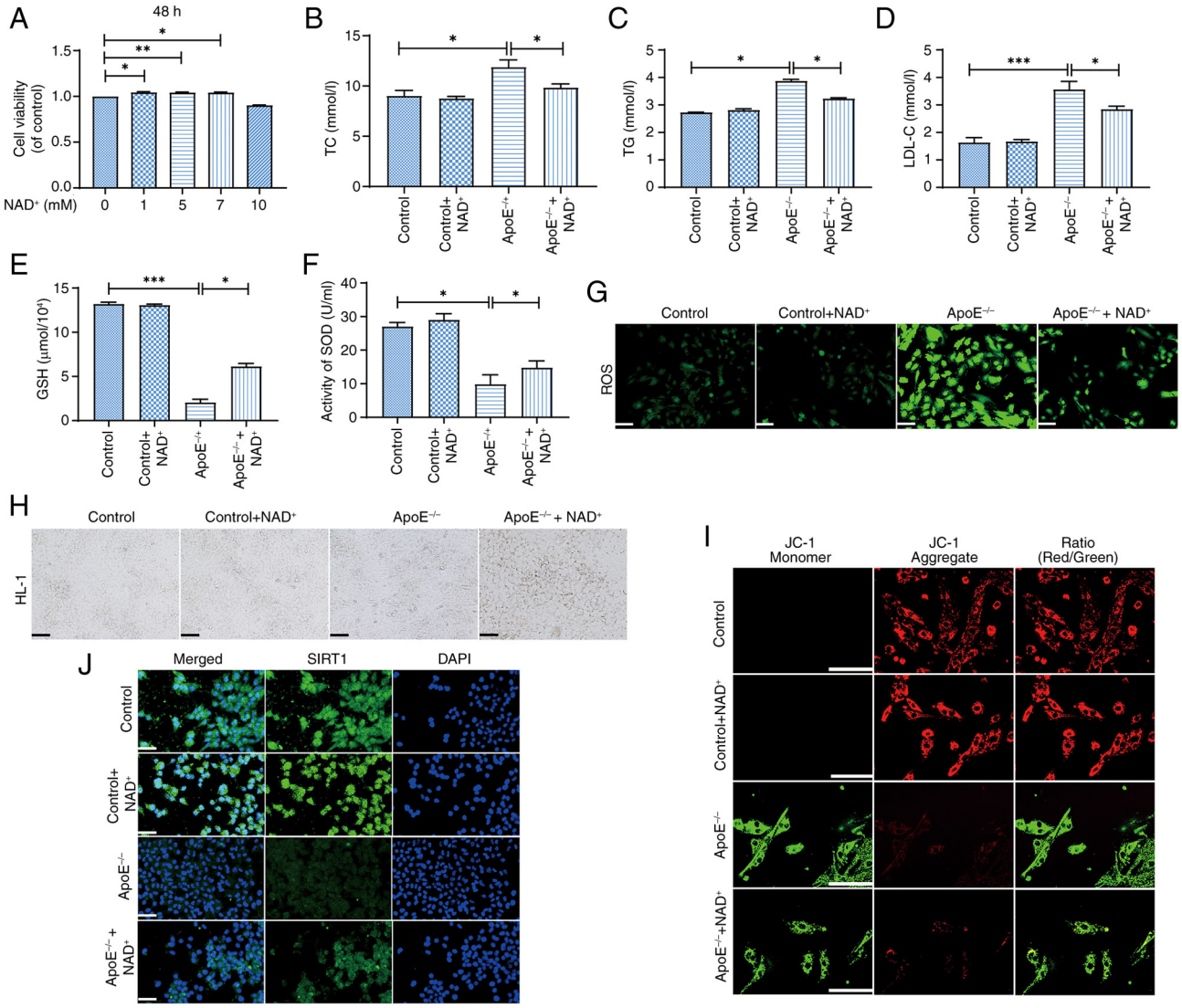

Figure 6. NAD^+ protects $ApoE^{-/-}$ HL-1 cells from lipid accumulation and oxidative stress. (A) Cell viability was significantly enhanced in the 5 mM NAD^+ group compared with that in the control group. (B) NAD^+ supplementation reduced TC levels in $ApoE^{-/-}$-treated cells. (C) TG levels were also significantly decreased by NAD^+ treatment. (D) LDL-C levels were also reduced in the $ApoE^{-/-}$ + NAD^+ group, indicating improved lipid metabolism. (E) NAD^+ supplementation increased GSH levels, reflecting enhanced antioxidant defense. (F) SOD activity was also significantly elevated in the $ApoE^{-/-}$ + NAD^+ group, suggesting improved oxidative stress response. (G) ROS staining revealed reduced reactive oxygen species in the $ApoE^{-/-}$ + NAD^+ group, indicating a decrease in oxidative stress. Scale bar, 200 μm. (H) Microscopic images confirmed improved cell morphology and viability in the $ApoE^{-/-}$ + NAD^+ group. Scale bar, 100 μm. (I) JC-1 staining showed improved mitochondrial membrane potential in the $ApoE^{-/-}$ + NAD^+ group. Scale bar, 100 μm. (J) Immunofluorescence staining demonstrated increased expression of SIRT1 in the $ApoE^{-/-}$ + NAD^+ group, suggesting activation of the SIRT1 pathway. Magnification, x40; scale bar, 50 μm. Data are presented as the mean ± standard error of the mean (n=3); statistical analysis was performed using one-way ANOVA followed by Tukey's post hoc test. $^*P<0.05$, $^{**}P<0.01$, $^{***}P<0.001$. $ApoE^{-/-}$, apolipoprotein E-deficient; GSH, glutathione; LDL-C, low-density lipoprotein cholesterol; NAD^+, nicotinamide adenine dinucleotide; ROS, reactive oxygen species; SIRT1, sirtuin 1; SOD, superoxide dismutase; TC, total cholesterol; TG, triglycerides.

and modulated p-mTOR levels altered by PA, indicative of enhanced autophagic flux; this effect was abolished by EX-527 Fig. S5). These results suggested that NAD^+ may exert its protective effects through functional activation of SIRT1.

The present findings support the notion that NAD^+ could promote autophagy in cardiomyocytes via the modulation of autophagic flux, potentially contributing to its cardioprotective effects. In addition, it was suggested that NAD^+ supplementation not only modulated the MFN2/SIRT1 pathway but also activated the PI3K/AKT signaling pathway, contributing to improved cellular function and mitochondrial integrity. Notably, NAD^+ did not produce significant effects on autophagy- or metabolism-related markers in untreated HL-1 cells, indicating that its regulatory role is specific to lipotoxic or stress-induced conditions (Fig. S6).

Discussion

The present study systematically investigated the effects of NAD^+ supplementation and exercise intervention on a model of HFD-induced cardiac injury, highlighting their key roles in alleviating oxidative stress, correcting metabolic dysfunction and modulating autophagy. $ApoE^{-/-}$ mice were selected as a model of hyperlipidemia and atherosclerosis. Owing to the lack of ApoE, these mice develop spontaneous hypercholesterolemia and exhibit early cardiovascular alterations

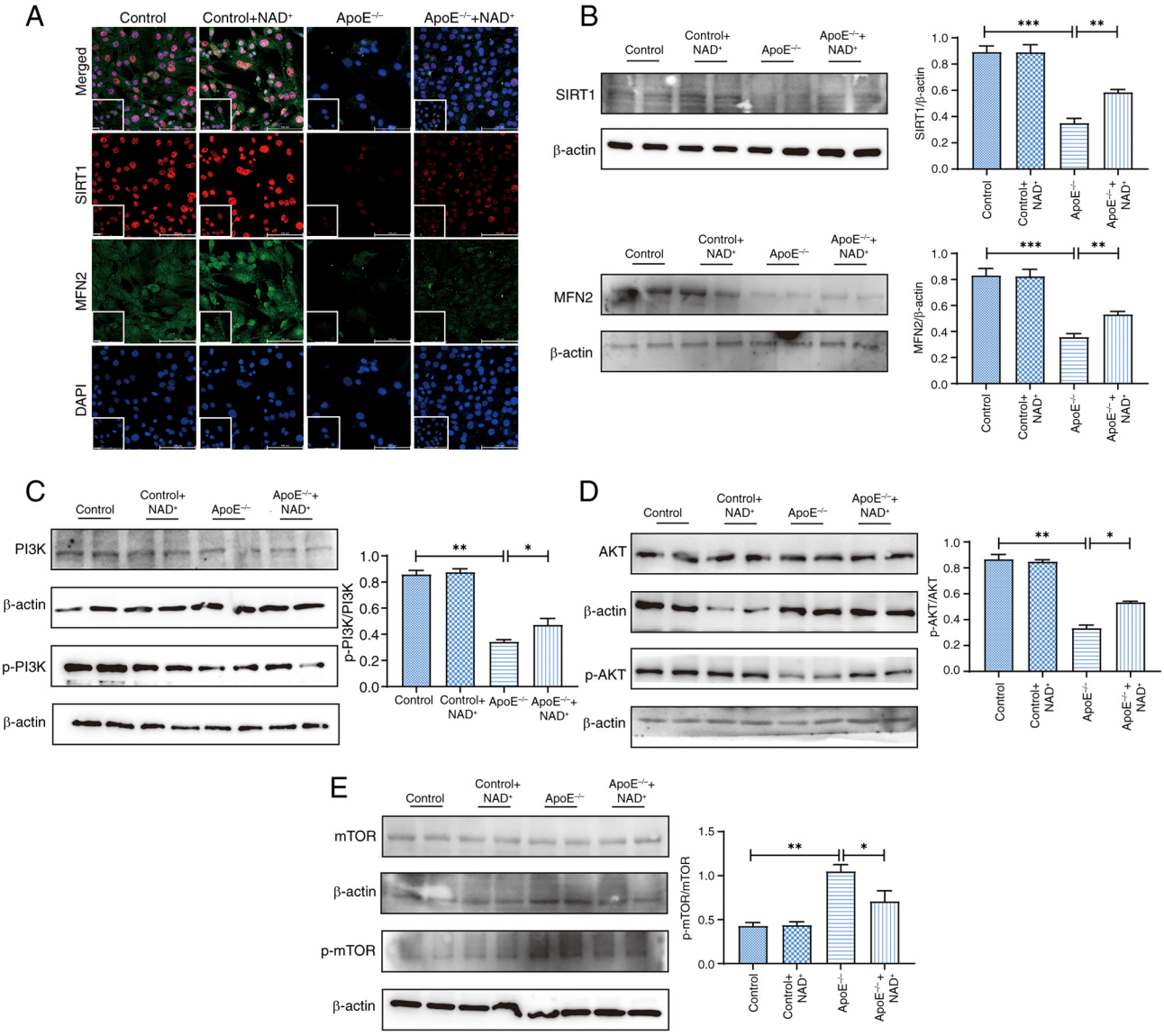

Figure 7. NAD+ enhances MFN2/SIRT1 expression and activates the PI3K/AKT pathway in HL-1 cells. (A) Representative immunofluorescence double staining showing colocalization of MFN2 and SIRT1 in HL-1 cells. Magnification, x40; scale bars, 100 and 50 μm. Protein expression levels of (B) SIRT1 and MFN2, (C) PI3K and p-PI3K, (D) AKT and p-AKT, and (E) mTOR and p-mTOR in HL-1 cells. Data are presented as the mean ± SEM (n=4); statistical analysis was performed using one-way ANOVA followed by Tukey's post hoc test. *P<0.05, **P<0.01, ***P<0.001. ApoE$^{-/-}$, apolipoprotein E-deficient; MFN2, mitofusin 2; NAD+, nicotinamide adenine dinucleotide; p-, phosphorylated; SIRT1, sirtuin 1.

under a HFD, closely resembling human cardiometabolic disorders (28,29). Notably, in the present study different HFD formulations and suppliers were used for each model; however, both diets were selected based on their validation in the literature for reliably inducing hyperlipidemia, obesity and cardiovascular dysfunction in rodents (30). Moreover, both suppliers are certified Chinese manufacturers whose products meet national standards for laboratory animal feed production; although minor compositional differences (such as fatty acid profiles and micronutrients) between diet sources could theoretically affect certain metabolic parameters, consistent phenotypic outcomes were observed in terms of body weight gain, serum lipid levels and cardiac pathology. These findings support the reproducibility and reliability of both models.

The present HFD model offered a sensitive and reproducible platform for evaluating interventions targeting lipid metabolism, oxidative stress and myocardial injury. Notably, ApoE$^{-/-}$ mice represent a hyperlipidemia-prone model with increased susceptibility to cardiac injury (31). This enabled the present study to delineate the cardioprotective effects of NAD+ under metabolic stress, particularly via activation of the SIRT1/MFN2 and PI3K/AKT/mTOR pathway. Future studies using wild-type mice should be performed to determine whether NAD+ confers similar benefits under physiological or less severe metabolic conditions, thereby assessing its broader translational potential (32,33). Unlike earlier studies relying on NAD+ precursors, the approach of the present study directly demonstrated the therapeutic value of NAD+ in lipid-induced myocardial injury (34,35).

Exercise is a well-recognized non-pharmacological intervention that improves metabolic homeostasis and cardiovascular health , and it has been shown to enhance endogenous NAD+ biosynthesis via AMPK and NAMPT pathways (36,37). In the present study, although the focus was on exogenous

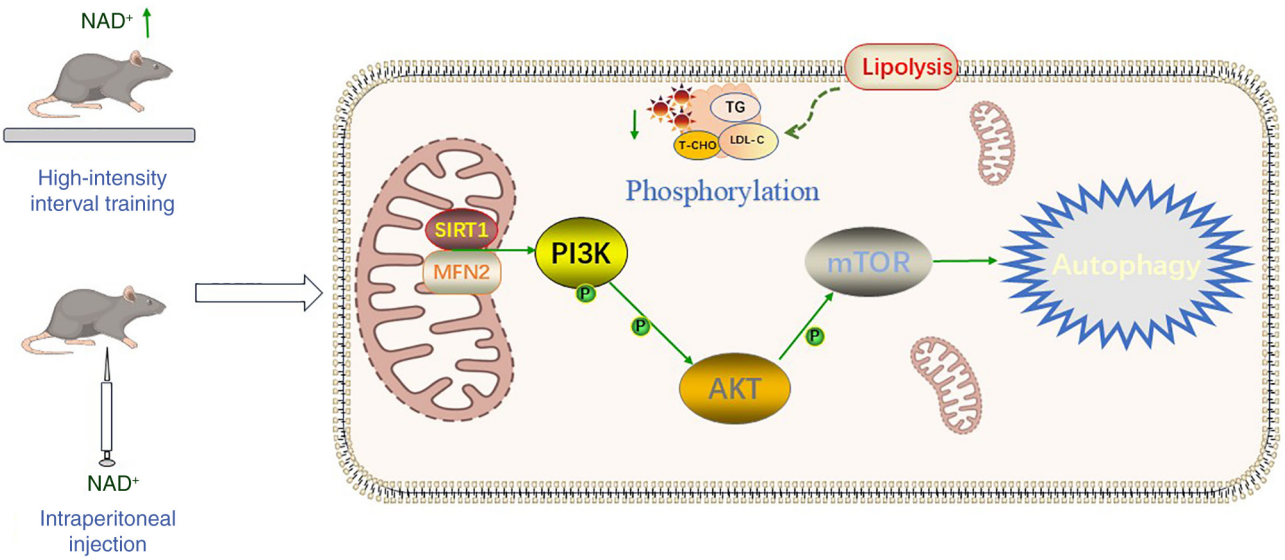

Figure 8. Mechanistic overview of NAD+ in improving HFD-induced cardiac dysfunction. High-intensity interval training elevates cardiac NAD+ levels, and subsequent intraperitoneal NAD+ supplementation further activates SIRT1/MFN2 signaling. This enhances PI3K/AKT/mTOR phosphorylation, promoting autophagy and mitochondrial quality control. Interventions also improve lipid metabolism, reducing TG, T-CHO, and LDL-C. Together, these mechanisms mitigate mitochondrial dysfunction, and metabolic disturbances in HFD-induced cardiac injury. LDL-C, low-density lipoprotein cholesterol; MFN2, mitofusin 2; NAD+, nicotinamide adenine dinucleotide; T-CHO, total cholesterol; TG, triglycerides; SIRT1, sirtuin 1.

NAD+ supplementation, the results revealed that HIIT also elevated cardiac NAD+ levels, and alleviated oxidative stress, fibrosis and myocardial injury in ApoE$^{-/-}$ mice. These results underscore the potential of exercise to mitigate hyperlipidemia-induced cardiac damage, partially through NAD+-related mechanisms. The findings demonstrated that NAD+ markedly improved mitochondrial integrity and reduced excessive ROS accumulation potentially by activating the SIRT1/MFN2 pathway (Fig. 8), thereby protecting cardiomyocytes from metabolic stress-induced damage. Furthermore, the combination of NAD+ and HIIT may amplify these protective effects by enhancing tissue NAD+/NADH ratios and increasing the phosphorylation levels of PI3K and AKT, thereby modulating the PI3K/AKT/mTOR signaling pathway and providing a multilayered cardioprotective mechanism at both molecular and cellular levels., providing a multilayered cardioprotective mechanism at both molecular and cellular levels. Although prior studies have explored the independent roles of NAD+ and exercise in cardiac metabolic regulation (38-40), the present study provides preliminary evidence suggesting that NAD+ supplementation combined with HIIT may exert complementary protective effects against HFD-induced cardiac damage, offering potential theoretical insights and therapeutic implications for metabolic cardiomyopathy.

SIRT1, a NAD+-dependent deacetylase, serves a central role in regulating mitochondrial function, oxidative stress and metabolic homeostasis (41). NAD+ supplementation markedly upregulated SIRT1 expression, thereby attenuating oxidative damage through enhanced mitochondrial quality control and reduced ROS generation. Additionally, SIRT1 deacetylates MFN2, a critical protein in mitochondrial fusion, stabilizing its function under metabolic stress conditions (42). In addition to the involvement of the SIRT1/MFN2 pathway, the present study demonstrated that exercise increased NAD+ levels, which subsequently activated the PI3K/AKT/mTOR signaling pathway via SIRT1/MFN2. This pathway is known to play a crucial role in regulating lipid accumulation, fibrosis, and metabolic homeostasis (43). Excessive activation of this pathway in HFD models has been associated with exacerbated cardiac remodeling. By suppressing this signaling cascade, NAD+ and exercise intervention effectively reduced myocardial fibrosis and lipid deposition. These findings align with previous metabolic studies and highlight the beneficial effects of NAD+ supplementation and exercise in improving metabolic cardiomyopathy (44,45).

The present study highlighted the distinct effects of HIIT and MICT on cardiac metabolic regulation. HIIT demonstrated superior benefits in increasing NAD+ levels and reducing oxidative stress compared with MICT. The acute metabolic stress induced by HIIT may trigger the activation of NAD+ biosynthetic enzymes such as NAMPT, thereby amplifying NAD availability and improving mitochondrial function (46,47). These findings underscore the potential of HIIT as a potent exercise modality for enhancing cardiac resilience in metabolic conditions. From a clinical perspective, the specificity of exercise interventions highlights the importance of tailoring training regimens to optimize therapeutic outcomes. Future studies should further explore the dose-response relationship of exercise intensity and NAD+ supplementation in improving cardiac function.

The involvement of SIRT1/MFN2 and PI3K/AKT/mTOR pathways offers mechanistic insights in heart and liver (42,48-50). The present findings build upon and expand the existing knowledge on the independent effects of NAD+ and exercise in cardiac metabolic regulation. Previous studies have predominantly investigated their individual effects. This dual approach amplifies the benefits, providing a more comprehensive understanding of how metabolic and mechanical interventions can jointly enhance cardiac health. To further validate the signaling relationship, *in vitro*

experiments were performed using the specific SIRT1 inhibitor EX-527 (51). Treatment with EX-527 significantly attenuated NAD^+-induced activation of the p-mTOR mTOR pathway, indicating that SIRT1 is an upstream regulator. These results confirm that the PI3K/AKT/mTOR pathway functions downstream of the SIRT1/MFN2 pathway. The additional experiments using EX-527 confirmed that SIRT1 modulates the PI3K/AKT/mTOR pathway in response to NAD^+, reinforcing the proposed SIRT1/MFN2-PI3K/AKT/mTOR signaling cascade involved in cardioprotection. Moreover, exogenous NAD^+ supplementation reduced the levels of LC3 II and P62 in the hyperlipidemia model, indicating that autophagic degradation may be restored and autophagic flow enhanced after NAD^+ supplementation. Therefore, it could be hypothesized that NAD^+ treatment promotes the maturation of autophagosomes and enhances the fusion of autophagosomes with lysosomes, thereby improving autophagic flow and promoting autophagic degradation in hyperlipidemia-induced heart injury. These findings establish a foundation for future translational studies exploring the broader applications of NAD^+ and exercise intervention.

In conclusion, the present study demonstrated that NAD^+ supplementation and exercise, particularly HIIT, independently protect against HFD-induced cardiac damage by targeting oxidative stress, mitochondrial dysfunction, and metabolic disturbances. The protective effects of NAD^+ in HFD-induced cardiac injury were mediated primarily via activation of the SIRT1/MFN2 pathway and the PI3K/AKT/mTOR pathway. These findings provide new insights into the prevention and treatment of metabolic cardiomyopathy, supporting further research and potential clinical applications.

Acknowledgements

Not applicable.

Funding

The present study was funded by the Central Hospital of Dalian University of Technology 'Climbing Plan' (grant no. 2023ZZ008).

Availability of data and materials

The data generated in the present study may be requested from the corresponding author.

Authors' contributions

ZP designed the study. SG and WY performed the experiments. ZP, SG and WY analyzed the data. ZP and SG confirm the authenticity of all the raw data. SG and WY drafted and wrote the manuscript. JY and YL analyzed the data and revised the manuscript. All authors read and approved the final manuscript.

Ethics approval and consent to participate

All animal experiments were performed in accordance with the Guide for the Care and Use of Laboratory Animals and were approved by the Ethics Committee of Dalian Municipal Central Hospital (grant no. YN2023-057-55).

Patient consent for publication

Not applicable.

Competing interests

The authors declare that they have no competing interests.

References

1. Kotseva K, Jennings C, Bassett P, Adamska A, Hobbs R and Wood D; ASPIRE-3-PREVENT Investigators: Challenge of cardiovascular prevention in primary care: Achievement of lifestyle, blood pressure, lipids and diabetes targets for primary prevention in England-results from ASPIRE-3-PREVENT cross-sectional survey. Open Heart 11: e002704, 2024.
2. Han S, Kim NR, Kang JW, Eun JS and Kang YM: Radial BMD and serum CTX-I can predict the progression of carotid plaque in rheumatoid arthritis: A 3-year prospective cohort study. Arthritis Res Ther 23: 258, 2021.
3. Zheng L, Than A, Zan P, Li D, Zhang Z, Leow MKS and Chen P: Mild-photothermal and nanocatalytic therapy for obesity and associated diseases. Theranostics 14: 5608-5620, 2024.
4. Narasimhulu CA and Singla DK: BMP-7 Attenuates sarcopenia and adverse muscle remodeling in diabetic mice via alleviation of lipids, inflammation, HMGB1, and pyroptosis. Antioxidants (Basel) 12: 331, 2023.
5. Galluzzi L, Vitale I, Aaronson SA, Abrams JM, Adam D, Agostinis P, Alnemri ES, Altucci L, Amelio I, Andrews DW, *et al*: Molecular mechanisms of cell death: Recommendations of the Nomenclature committee on cell death 2018. Cell Death Differ 25: 486-541, 2018.
6. Shoji S and Mentz RJ: Beyond quadruple therapy: The potential roles for ivabradine, vericiguat, and omecamtiv mecarbil in the therapeutic armamentarium. Heart Fail Rev 29: 949-955, 2024.
7. Bentivegna E, Galastri S, Onan D and Martelletti P: Unmet needs in the acute treatment of migraine. Adv Ther 41: 1-13, 2024.
8. Perryman R, Chau TW, De-Felice J, O'Neill K and Syed N: Distinct capabilities in NAD metabolism mediate resistance to NAMPT inhibition in glioblastoma. Cancers (Basel) 16: 2054, 2024.
9. Abdellatif M, Sedej S and Kroemer G: NAD^+ metabolism in cardiac health, aging, and disease. Circulation 144: 1795-1817, 2021.
10. Chu X and Raju RP: Regulation of NAD(+) metabolism in aging and disease. Metabolism 126: 154923, 2022.
11. Lin Q, Zuo W, Liu Y, Wu K and Liu Q: NAD(+) and cardiovascular diseases. Clin Chim Acta 515: 104-110, 2021.
12. Yoshino M, Yoshino J, Kayser BD, Patti GJ, Franczyk MP, Mills KF, Sindelar M, Pietka T, Patterson BW, Imai SI and Klein S: Nicotinamide mononucleotide increases muscle insulin sensitivity in prediabetic women. Science 372: 1224-1229, 2021.
13. Cheng L, Deepak RNVK, Wang G, Meng Z, Tao L, Xie M, Chi W, Zhang Y, Yang M, Liao Y, *et al*: Hepatic mitochondrial NAD + transporter SLC25A47 activates AMPKα mediating lipid metabolism and tumorigenesis. Hepatology 78: 1828-1842, 2023.
14. Lopaschuk GD, Karwi QG, Tian R, Wende AR and Abel ED: Cardiac energy metabolism in heart failure. Circ Res 128: 1487-1513, 2021.
15. Doan KV, Luongo TS, Ts'olo TT, Lee WD, Frederick DW, Mukherjee S, Adzika GK, Perry CE, Gaspar RB, Walker N, *et al*: Cardiac NAD^+ depletion in mice promotes hypertrophic cardiomyopathy and arrhythmias prior to impaired bioenergetics. Nat Cardiovasc Res 3: 1236-1248, 2024.
16. Qiu Y, Xu S, Chen X, Wu X, Zhou Z, Zhang J, Tu Q, Dong B, Liu Z, He J, *et al*: NAD(+) exhaustion by CD38 upregulation contributes to blood pressure elevation and vascular damage in hypertension. Signal Transduct Target Ther 8: 353, 2023.
17. Li J, Zhang C, Hu Y, Peng J, Feng Q and Hu X: Nicotinamide enhances Treg differentiation by promoting Foxp3 acetylation in immune thrombocytopenia. Br J Haematol 205: 2432-2441, 2024.

18. Pei Z, Wang F, Wang K and Wang L: Nicotinamide adenine dinucleotide in the development and treatment of cardiac remodeling and aging. Mini Rev Med Chem 22: 2310-2317, 2022.
19. Fritzen AM, Lundsgaard AM and Kiens B: Tuning fatty acid oxidation in skeletal muscle with dietary fat and exercise. Nat Rev Endocrinol 16: 683-696, 2020.
20. Qi XM, Qiao YB, Zhang YL, Wang AC, Ren JH, Wei HZ and Li QS: PGC-1α/NRF1-dependent cardiac mitochondrial biogenesis: A druggable pathway of calycosin against triptolide cardiotoxicity. Food Chem Toxicol 171: 113513, 2023.
21. Zhang H, Wang Y, Wu K, Liu R, Wang H, Yao Y, Kvietys P and Rui T: miR-141 impairs mitochondrial function in cardiomyocytes subjected to hypoxia/reoxygenation by targeting Sirt1 and MFN2. Exp Ther Med 24: 763, 2022.
22. Ji LL and Yeo D: Maintenance of NAD+ homeostasis in skeletal muscle during aging and exercise. Cells 11: 710, 2022.
23. National Research Council Committee for the Update of the Guide for the C. and A. Use of Laboratory. The National Academies Collection: Reports funded by National Institutes of Health, in Guide for the Care and Use of Laboratory Animals. National Academies Press, Washington, DC, 2011.
24. Nishida Y, Nawaz A, Kado T, Takikawa A, Igarashi Y, Onogi Y, Wada T, Sasaoka T, Yamamoto S, Sasahara M, *et al*: Astaxanthin stimulates mitochondrial biogenesis in insulin resistant muscle via activation of AMPK pathway. J Cachexia Sarcopenia Muscle 11: 241-258, 2020.
25. Brault V, Duchon A, Romestaing C, Sahun I, Pothion S, Karout M, Borel C, Dembele D, Bizot JC, Messaddeq N, *et al*: Opposite phenotypes of muscle strength and locomotor function in mouse models of partial trisomy and monosomy 21 for the proximal Hspa13-App region. PLoS Genet 11: e1005062, 2015.
26. Wang L, Lavier J, Hua W, Wang Y, Gong L, Wei H, Wang J, Pellegrin M, Millet GP and Zhang Y: High-Intensity interval training and moderate-intensity continuous training attenuate oxidative damage and promote myokine response in the skeletal muscle of ApoE KO mice on high-fat diet. Antioxidants (Basel) 10: 992, 2021.
27. Pei Z, Li Y, Yao W, Sun F and Pan X: NAD^+ Protects against hyperlipidemia-induced kidney injury in apolipoprotein E-deficient mice. Cur Pharm Biotechnol 25: 488-498, 2024.
28. Aravani D, Kassi E, Chatzigeorgiou A and Vakrou S: Cardiometabolic syndrome: An update on available mouse models. Thromb Haemost 121: 703-715, 2021.
29. Poledne R and Jurčíková-Novotná L: Experimental models of hyperlipoproteinemia and atherosclerosis. Physiol Res 66 (Suppl 1): S69-S75, 2017.
30. Park Y, Jang I, Park HY, Kim J and Lim K: Hypoxic exposure can improve blood glycemic control in high-fat diet-induced obese mice. Phys Act Nutr 24: 19-23, 2020.
31. Zhao Y, Qu H, Wang Y, Xiao W, Zhang Y and Shi D: Small rodent models of atherosclerosis. Biomed Pharmacother 129: 110426, 2020.
32. Zhao Y, Zhang J, Zheng Y, Zhang Y, Zhang XJ, Wang H, Du Y, Guan J, Wang X and Fu J: NAD^+ improves cognitive function and reduces neuroinflammation by ameliorating mitochondrial damage and decreasing ROS production in chronic cerebral hypoperfusion models through Sirt1/PGC-1α pathway. J Neuroinflammation 18: 207, 2021.
33. Guo C, Huang Q, Wang Y, Yao Y, Li J, Chen J, Wu M, Zhang Z, Mingyao E, Qi H, *et al*: Therapeutic application of natural products: NAD^+ metabolism as potential target. Phytomedicine 114: 154768, 2023.
34. Trueblood NA, Ramasamy R, Wang LF and Schaefer S: Niacin protects the isolated heart from ischemia-reperfusion injury. Am J Physiol Heart Circ Physiol 279: H764-H771, 2000.
35. Perry CE, Halawani SM, Mukherjee S, Ngaba LV, Lieu M, Lee WD, Davis JG, Adzika GK, Bebenek AN, Bazianos DD, *et al*: NAD+ precursors prolong survival and improve cardiac phenotypes in a mouse model of Friedreich's Ataxia. JCI Insight 9: e177152, 2024.
36. Chong MC, Silva A, James PF, Wu SSX and Howitt J: Exercise increases the release of NAMPT in extracellular vesicles and alters NAD^+ activity in recipient cells. Aging Cell 21: e13647, 2022.
37. Morales-Alamo D and Calbet JAL: AMPK signaling in skeletal muscle during exercise: Role of reactive oxygen and nitrogen species. Free Radic Biol Med 98: 68-77, 2016.
38. Glancy B, Kane DA, Kavazis AN, Goodwin ML, Willis WT and Gladden LB: Mitochondrial lactate metabolism: History and implications for exercise and disease. J Physiol 599: 863-888, 2021.
39. Agorrody G, Peclat TR, Peluso G, Gonano LA, Santos L, van Schooten W, Chini CCS, Escande C, Chini EN and Contreras P: Benefits in cardiac function by CD38 suppression: Improvement in NAD^+ levels, exercise capacity, heart rate variability and protection against catecholamine-induced ventricular arrhythmias. J Mol Cell Cardiol 166: 11-22, 2022.
40. Cabrera ME, Zhou L, Stanley WC and Saidel GM: Regulation of cardiac energetics: role of redox state and cellular compartmentation during ischemia. Ann N Y Acad Sci 1047: 259-270, 2005.
41. Chen Y, Zhang H, Ji S, Jia P, Chen Y, Li Y and Wang T: Resveratrol and its derivative pterostilbene attenuate oxidative stress-induced intestinal injury by improving mitochondrial redox homeostasis and function via SIRT1 signaling. Free Radic Biol Med 177: 1-14, 2021.
42. Hu L, Guo Y, Song L, Wen H, Sun N, Wang Y, Qi B, Liang Q, Geng J, Liu X, *et al*: Nicotinamide riboside promotes Mfn2-mediated mitochondrial fusion in diabetic hearts through the SIRT1-PGC1α-PPARα pathway. Free Radic Biol Med 183: 75-88, 2022.
43. Wu YC, Yan Q, Yue SQ, Pan LX, Yang DS, Tao LS, Wei ZY, Rong F, Qian C, Han MQ, *et al*: NUP85 alleviates lipid metabolism and inflammation by regulating PI3K/AKT signaling pathway in nonalcoholic fatty liver disease. Int J Biol Sci 20: 2219-2235, 2024.
44. Yu H, Gan D, Luo Z, Yang Q, An D, Zhang H, Hu Y, Ma Z, Zeng Q, Xu Z and Ren D: α-Ketoglutarate improves cardiac insufficiency through NAD(+)-SIRT1 signaling-mediated mitophagy and ferroptosis in pressure overload-induced mice. Mol Med 30: 15, 2024.
45. Ma Y, Kuang Y, Bo W, Liang Q, Zhu W, Cai M and Tian Z: Exercise training alleviates cardiac fibrosis through increasing fibroblast growth factor 21 and regulating TGF-β1-Smad2/3-MMP2/9 signaling in mice with myocardial infarction. Int J Mol Sci 22: 12341, 2021.
46. Walzik D, Joisten N, Schenk A, Trebing S, Schaaf K, Metcalfe AJ, Spiliopoulou P, Hiefner J, McCann A, Watzl C, *et al*: Acute exercise boosts NAD(+) metabolism of human peripheral blood mononuclear cells. Brain Behav Immun 123: 1011-1023, 2024.
47. Yagi M, Toshima T, Amamoto R, Do Y, Hirai H, Setoyama D, Kang D and Uchiumi T: Mitochondrial translation deficiency impairs NAD(+) -mediated lysosomal acidification. EMBO J 40: e105268, 2021.
48. Li J, Wang T, Liu P, Yang F, Wang X, Zheng W and Sun W: Hesperetin ameliorates hepatic oxidative stress and inflammation via the PI3K/AKT-Nrf2-ARE pathway in oleic acid-induced HepG2 cells and a rat model of high-fat diet-induced NAFLD. Food Funct 12: 3898-3918, 2021.
49. Savova MS, Mihaylova LV, Tews D, Wabitsch M and Georgiev M: Targeting PI3K/AKT signaling pathway in obesity. Biomed Pharmacother 159: 114244, 2023.
50. Magaye RR, Savira F, Hua Y, Xiong X, Huang L, Reid C, Flynn BL, Kaye D, Liew D and Wang BH: Attenuating PI3K/Akt- mTOR pathway reduces dihydrosphingosine 1 phosphate mediated collagen synthesis and hypertrophy in primary cardiac cells. Int J Biochem Cell Biol 134: 105952, 2021s.
51. Wawruszak A, Luszczki J, Bartuzi D, Kalafut J, Okon E, Czerwonka A and Stepulak A: Selisistat, a SIRT1 inhibitor, enhances paclitaxel activity in luminal and triple-negative breast cancer: In silico, in vitro, and in vivo studies. J Enzyme Inhib Med Chem 40: 2458554, 2025.